



**HAL**  
open science

## **ABACO-2: a comprehensive model for microalgae-bacteria consortia validated outdoor at pilot-scale**

Rebecca Nordio, Enrique Rodríguez-Miranda, Francesca Casagli, Ana  
Sánchez-Zurano, José Luis Guzmán, Gabriel Acién

► **To cite this version:**

Rebecca Nordio, Enrique Rodríguez-Miranda, Francesca Casagli, Ana Sánchez-Zurano, José Luis Guzmán, et al.. ABACO-2: a comprehensive model for microalgae-bacteria consortia validated outdoor at pilot-scale. *Water Research*, 2024, 248, pp.120837. 10.1016/j.watres.2023.120837. hal-04397215

**HAL Id: hal-04397215**

**<https://inria.hal.science/hal-04397215>**

Submitted on 16 Jan 2024

**HAL** is a multi-disciplinary open access archive for the deposit and dissemination of scientific research documents, whether they are published or not. The documents may come from teaching and research institutions in France or abroad, or from public or private research centers.

L'archive ouverte pluridisciplinaire **HAL**, est destinée au dépôt et à la diffusion de documents scientifiques de niveau recherche, publiés ou non, émanant des établissements d'enseignement et de recherche français ou étrangers, des laboratoires publics ou privés.



Distributed under a Creative Commons Attribution 4.0 International License

1 **ABACO-2: a comprehensive model for microalgae-bacteria consortia validated outdoor at**  
2 **pilot-scale**

3 Rebecca Nordio<sup>a,b</sup>, Enrique Rodríguez-Miranda<sup>b,c</sup>, Francesca Casagli<sup>d</sup>, Ana Sánchez-Zurano<sup>a,b</sup>,  
4 José Luis Guzmán<sup>b,c</sup>, Gabriel Ación<sup>a,b</sup>

5 <sup>a</sup> Department of Chemical Engineering, Universidad de Almería, E04120 Almería, Spain.

6 <sup>b</sup> CIESOL Solar Energy Research Centre, Joint Centre University of Almería-CIEMAT, 04120  
7 Almería, Spain.

8 <sup>c</sup> Department of Informatics, Universidad de Almería, E04120 Almería, Spain.

9 <sup>d</sup> Biocore, INRIA centre d'Université Côte d'Azur, Sophia-Antipolis F-06902, France.

10

11 \* **Corresponding author:** Rebecca Nordio, [rnordio@ual.es](mailto:rnordio@ual.es)

12

13 **Abstract**

14 Modelling microalgae-bacteria in wastewater treatment systems has gained significant attention in  
15 the last few years. In this study, we present an enhanced version of the ABACO model, named  
16 ABACO-2, which demonstrates improved accuracy through validation in outdoor pilot-scale systems.  
17 ABACO-2 enables the comprehensive characterization of microalgae-bacteria consortia dynamics,  
18 allowing to predict the biomass concentration (microalgae, heterotrophic bacteria, and nitrifying  
19 bacteria) and nutrient evolution. The updated version of the model incorporates new equations for  
20 nutrient coefficient yields, oxygen mass balance, and microorganism cellular decay, while  
21 significantly reducing the number of calibrated parameters, simplifying the parameter identification.  
22 Calibration and validation were performed using data from a 80 m<sup>2</sup> raceway reactor operated in a  
23 semicontinuous mode over an extensive period (May to November, total of 206 days) at a fixed  
24 dilution rate of 0.2 day<sup>-1</sup> (corresponding to 5 days of hydraulic retention time), where untreated urban  
25 wastewater was used as culture medium. ABACO-2 exhibited robustness, accurately forecasting  
26 biomass production, population dynamics, nutrient recovery, and prevailing culture conditions across  
27 a wide range of environmental and water composition conditions. Mathematical models are essential  
28 instruments for the industrial development and optimization of microalgae-related wastewater  
29 treatment processes, thereby contributing to the sustainability of the wastewater treatment industry.

30

31

32 **KEYWORDS:** Microalgae, wastewater, modeling

33

## 34 **1. Introduction**

35 Water reuse and recycling have become crucial topics of discussion in recent decades, owing to  
36 their significant environmental and social implications. With rapid industrialization and population  
37 growth, the volume of wastewater generated annually has escalated (Angelakis and Gikas, 2014).  
38 contributing to water stress in various regions worldwide, particularly in southern Europe, including  
39 Spain, Italy, and Greece (Strosser et al., 2012). Consequently, researchers have directed their efforts  
40 toward developing innovative water remediation technologies. Among these technologies,  
41 microalgae-based wastewater systems have emerged as a promising solution, capable of replacing  
42 traditional secondary and tertiary classical wastewater treatment processes (Abdel-Raouf et al.,  
43 2012). The utilization of microalgae in water remediation offers several advantages. Firstly, it  
44 demands less energy compared to conventional methods. Secondly, it significantly reduces  
45 greenhouse gas emissions. Additionally, microalgae systems eliminate residues effectively and yield  
46 valuable biomass, which can be utilized in various industrial applications (Mohd Udaiyappan et al.,  
47 2017).

48 Microalgae are photosynthetic microorganisms capable of using CO<sub>2</sub> as a carbon source and light  
49 as an energy source, in addition to using nitrogen (N) and phosphorus (P) present in wastewater to  
50 produce biomass. Moreover, thanks to the presence of bacteria, the organic matter's degradation is  
51 ensured (Muñoz and Guieysse, 2006). The effectiveness of microalgae-based wastewater systems  
52 has been demonstrated through pilot-scale testing in raceway reactors (Morillas-España et al.,  
53 2021b) and thin layers (Grivalský et al., 2019). These studies have proven that these systems are  
54 robust and reliable, enabling the recovery of nutrients from wastewater and producing treated water  
55 that meets the regulatory standards set by European legislation (Council Directive of May 1991  
56 concerning urban wastewater treatment, 1991). One of the key factors contributing to the success  
57 of this technology is its resilience in the face of significant variations in water composition and  
58 weather conditions (Nordio et al., 2023). However, high costs and relatively low efficiency are  
59 foreclosing the entire industrial development of these systems (Acién et al., 2014). The industrial  
60 development of these processes can be possible only after the improved understanding and

61 optimized management of the biological system allowing to study which are the main parameters  
62 influencing biomass productivity and the water remediation capacity (Solimeno and García, 2017).

63 In this framework, mathematical modelling serves as a valuable tool for describing these processes;  
64 as it enables simulations and performance evaluations under different environmental and process  
65 conditions, aiding optimization and the development of control strategies (Solimeno and García,  
66 2017). In the literature, it is possible to find many examples of microalgae models that evaluate the  
67 growth rate as a function mainly of light, temperature, nutrients and pH (Lee et al., 2015). On the  
68 contrary, a few examples of comprehensive models for microalgae-based wastewater treatments  
69 are available, defined as models that consider the effect of multiple process parameters and  
70 biological mechanisms. Examples of recent comprehensive models are the Zambrano model  
71 (Zambrano et al., 2016), the BIOALGAE model (Solimeno et al., 2019), and the ALBA model (Casagli  
72 et al., 2021). Nevertheless, it is challenging to obtain validation data over an extended period and  
73 using urban wastewater in industrial facilities, so in the literature, some alternatives can be found,  
74 such as validations achieved with digestates, synthetic waters, or small-scale reactors. However, it  
75 is crucial to develop models that accurately represent the biological system in real conditions (both  
76 environmental and operational) since they are intended for use in commercial wastewater treatment  
77 facilities. In Spain, for example, there are currently four industrial facilities using microalgae for urban  
78 wastewater treatment, employing reactors ranging from 0.5 to 1.0 ha (Masojidek et al., 2022).

79 To apply these models to large-scale production, it is important to balance complexity and realism.  
80 For instance, very complex mathematical descriptions of all the metabolic reactions involved in  
81 photosynthesis, may not improve the model prediction accuracy, compared to the computational  
82 cost required. Additionally, mechanisms that are not relevant for long-time series and continuous  
83 conditions can be omitted from the model (Darvehei et al., 2018). Furthermore, in wastewater,  
84 thousands of bacterial groups can interact with microalgae, and it is fundamental to carefully select  
85 the most relevant groups to reduce the number of equations and the overall complexity. Generally,  
86 only a few groups are considered relevant, as they influence nutrient uptake from the culture  
87 medium. The first model was proposed by Buhr & Miller in 1983 (Buhr and Miller, 1983), for example,

88 only two populations (algae and aerobic bacteria) were considered. However, afterwards, the leading  
89 bacterial groups identified were the heterotrophic bacteria, which permitted the oxidation of the  
90 organic matter, and nitrifying bacteria that compete with microalgae for the consumption of nitrogen  
91 (together with phosphorous and carbon) in some cases distinguished between ammonia-oxidizing  
92 bacteria (AOB) and nitrite-oxidizing bacteria (NOB) (Aparicio et al., 2022a).

93 In this work, an improved version of the ABACO model (Sánchez-zurano et al., 2021), named the  
94 ABACO-2 model is proposed, calibrated and validated for outdoor conditions. Specifically, new  
95 equations are included to reduce the number of calibrated parameters, and the use of the oxygen  
96 mass balance allows for improvement in the accuracy of the model. Equations have been  
97 implemented using Python language and numpy packages while the calibration has been carried  
98 out with Scipy library and the optimization tool that uses the "Nelder-Mead" algorithm. The model  
99 has been validated over an extensive period (May-November); data have been collected from a  
100 demonstrative pilot-scale raceway reactor of 12 m<sup>3</sup> (80 m<sup>2</sup>) on which the prevailing strain was  
101 *Scenedesmus sp.*. The reactor was operated in semi-continuous mode at a fixed rate of 0.2 day<sup>-1</sup>  
102 using urban wastewater as culture medium. For this study, wastewater not pre-treated besides the  
103 removal of large particles was used, so subjected to high variation in terms of composition. This  
104 large variability of water nutrient concentration, together with different values of solar radiation and  
105 temperature typical of different year seasons, allowed to calibrate and validate the model in a wide  
106 range of conditions (Section 2.2), so increasing its prediction accuracy and robustness.

## 107 **2. Material and methods**

### 108 **2.1. Raceway reactor and inoculum**

109 Experimental data were collected from an 80 m<sup>2</sup> (12 m<sup>3</sup>) raceway reactor working in semi-continuous  
110 mode between April and December, with a fixed dilution rate of 0.2 day<sup>-1</sup>. The raceway was installed  
111 in the SABANA Demo Plant located in the IFAPA research centre in La Cañada, Almería, Spain. It  
112 was composed of a double channel of 40 m and a sump of 0.59 m<sup>3</sup> for the gas injections through  
113 diffusers and an electric motor connected to a paddlewheel system for culture mixing. The pH was  
114 monitored through sensors and controlled through CO<sub>2</sub> injection in the reactor sump. Additionally,

115 an independent airflow allowed reducing the concentration of dissolved oxygen. The culture depth  
116 was fixed at 0.15 m. In order to thoroughly monitor the culture dynamics, additional sensors have  
117 been installed for recording the dissolved oxygen (0-400% Sat), pH (0-14), temperature (0-80°C)  
118 and culture depth (4-40 cm). Moreover, a meteorological station allowed for registering the weather  
119 conditions regarding solar radiation and environmental temperature.

120 The chosen inoculum was *Scenedemus sp.* because it was demonstrated to be suitable microalgae  
121 that can easily be grown in wastewater and a wide range of conditions (Fernández Sevilla et al.,  
122 2006). The strain was initially grown on a fertilizer medium (0.9 g·L<sup>-1</sup> of NaNO<sub>3</sub>, 0.18 g·L<sup>-1</sup> of MgSO<sub>4</sub>,  
123 0.14 g·L<sup>-1</sup> of KH<sub>2</sub>PO<sub>4</sub> and 0.003 g·L<sup>-1</sup> of Kerantol), first using columns of 0.1 m<sup>3</sup> and then in a tubular  
124 system of 3 m<sup>3</sup> until it reached the concentration of 1 g·L<sup>-1</sup>. The biomass was then used as inoculum  
125 for the raceways. The culture was diluted with wastewater and kept in batch mode for one week,  
126 after that being operated in semi-continuous mode until it reached a stable biomass concentration  
127 (approximating a steady state condition).

## 128 **2.2. Environmental conditions and water composition**

129 As previously mentioned, environmental conditions in terms of temperature and radiation were  
130 continuously recorded throughout the entire period. The Photosynthetically Active Radiation (PAR)  
131 registered were ranged from 2000 μE·m<sup>-2</sup>·s<sup>-1</sup> during the months of April and May, gradually  
132 decreasing during the colder seasons with peaks at 1200 μE·m<sup>-2</sup>·s<sup>-1</sup>, with an average of 620 μE·m<sup>-2</sup>·s<sup>-1</sup>  
133 and 350 μE·m<sup>-2</sup>·s<sup>-1</sup> respectively. Regarding temperature, the highest values were recorded  
134 during the summer season (July-August), reaching peaks of 38°C, while in the spring season (April-  
135 May), they ranged between 25-35 °C, and in the autumn season (September-November), between  
136 25-12 °C.

137 Regarding the culture medium, it consisted of wastewater collected from the University of Almería  
138 during the entire data collection period, except for August when the water was sourced from the  
139 primary water treatment plant in the city of Almeria. In both instances, the water underwent pre-  
140 treatment, involving the removal of solid particles through an industrial filter (Azud Helix, 200 μm),  
141 before being introduced into the culture. During the study period, the nutrient concentration of the

142 wastewater varied over a wide range. Specifically, ammonium ( $\text{NH}_4^+$ ) concentration varies between  
143  $10 - 400 \text{ g}\cdot\text{m}^{-3}$ , nitrate ( $\text{NO}_3^-$ ) concentration ranged from  $0 - 13 \text{ g}\cdot\text{m}^{-3}$ , phosphate ( $\text{PO}_4^{2-}$ ) between  $30$   
144  $- 76 \text{ g}\cdot\text{m}^{-3}$ , while the chemical oxygen demand (COD) between  $100 - 600 \text{ gO}_2\cdot\text{m}^{-3}$ .

### 145 **2.3. Biomass concentration and nutrients analysis**

146 The influent wastewater and the filtered effluent were analysed in terms of nutrient content (N- $\text{NO}_3^-$ ,  
147 N- $\text{NH}_4^+$ , P- $\text{PO}_4^{3-}$ ) and COD. The biomass concentration in the culture was daily measured through  
148 the dry weight (DW) method. The culture was collected in the morning after the reactor sump, and  
149  $100 \text{ mL}$  were filtered in a  $0.5 \mu\text{m}$  filter and let dry for  $24\text{h}$  at  $80^\circ\text{C}$  in an oven. Regarding the nutrients,  
150 they were analysed through colourimetric methodologies in a spectrophotometer according to  
151 standard procedures (Standard IC 74246, Standard IC 38364, Standard IC 59755). The total COD  
152 was measured with Hanch-Lange kits (LCI-400) and the biodegradable soluble organic matter  
153 (BSMO) was estimated as a percentage of the total COD as reported in the literature by Pasztor I.  
154 et al., 2009.

### 155 **2.4. Data collection and analysis**

156 Experimental online data were collected every second by a set of sensors, connected to a  
157 Programming Logic Controller (PLC) and a Supervisory Control and Data Acquisition (SCADA)  
158 system. On the contrary, data coming from laboratory analysis as described in the previous section,  
159 were collected once a day. Given the big amount of data available, it was necessary to perform a  
160 prior data analysis following a procedure inspired by the “Cross Industry Standard Process Alliance  
161 for Data Mining” (CRISP-DM) approach (Ncr and Clinton, 1999). This methodology is one of the  
162 most used among data mining problems and it is composed of six main steps: (i) Business  
163 understanding, (ii) Data understanding, (iii) Data preparation, (iv) Modelling, (v) Evaluation, and (vi)  
164 Deployment. In this research, the first five steps have been developed as briefly described below:

165 I. Business understanding: the objective is to develop a model that can describe the evolution  
166 of microalgae-bacteria populations in wastewater-related systems. The aim is to develop a



167 tool that allows the simulation of the variation of biomass and nutrient concentration with time  
168 as a function of environmental and process parameters.

169 II. Data understanding: data have been collected as described in the previous section, studied,  
170 and analysed.

171 III. Data preparation: Datasets have been ordered, cleaned, and prepared for the modelling step.

172 IV. Modelling: the biological system has been modelled as described in the next sections.  
173 Stepping back to data preparation is often necessary. A part of the experimental data set has  
174 been used for the identification of the calibration parameters.

175 V. Evaluation: the developed model has been validated with long-term outdoor dataset. If the  
176 quality of the model was not enough to reach the defined objective, the data preparation and  
177 modelling part has been reviewed.

178 VI. Deployment: this step was not addressed in this research. However, a web interface for  
179 model utilization will be developed in future works.

### 180 **3. Model development**

#### 181 **3.1. Model concept**

182 This work considers three microbial groups: microalgae, heterotrophic bacteria and nitrifying bacteria  
183 as they are the main actors in the nutrient uptake and the  $O_2/CO_2$  fluxes (Figure 1). During the day,  
184 microalgae perform photosynthesis consuming the inorganic carbon and fixing nitrogen and  
185 phosphorus while producing  $O_2$ . The preferred nitrogen form for microalgae growth is  $NH_4^+$ , which is  
186 highly present in urban wastewater. Microalgae compete with nitrifying bacteria for the uptake of this  
187 compound since they use it to transform it into  $NO_3^-$  during the nitrification. The nitrification process  
188 involved the oxidation of  $NH_4^+$  to  $NO_2^-$  by AOB and then NOB transform  $NO_2^-$  into  $NO_3^-$ . For this  
189 study, it is considered that the nitrification is complete because it was not registered a significant  
190 concentration of  $NO_2^-$  in the culture (consistently below  $5\text{ g}\cdot\text{m}^{-3}$ ). Moreover, microalgae can use  $NO_3^-$   
191 as a form of nitrogen, but its consumption takes place only when ammonium is found below a given  
192 threshold (prior experimental analysis have estimated it as  $80\text{ g}\cdot\text{m}^{-3}$ ). Heterotrophic bacteria are  
193 considered the leading bacteria group as they are the main ones responsible for the degradation of  
194 organic matter. For the present work, the COD has been fractionated as proposed by Pasztor I. et

195 al., 2009. Briefly, the total COD can be divided into two main fractions: the biodegradable (readily  
196 and slowly) and the non-biodegradable (soluble and particulate). Heterotrophic bacteria can  
197 consume only the readily biodegradable organic matter estimated as 22% of the total COD and it  
198 will be called BSMO (biodegradable soluble organic matter) in this work. Summarizing, the BSMO  
199 concentration is decreased in the culture due to the heterotroph's activity and it can be increased  
200 due to the cellular death and decay of the microorganisms present in the culture. Regarding the gas  
201 fluxes, the inorganic carbon necessary for microalgae growth is partially provided by the on-demand  
202 injection of CO<sub>2</sub> for pH control and the natural release of CO<sub>2</sub> given by bacteria during respiration.  
203 This study assumes that microalgae are never limited by inorganic carbon concentration, as CO<sub>2</sub>  
204 injection always ensures enough carbon availability for microalgal growth, as already demonstrated  
205 by previous studies (Posadas et al., 2015). Additionally, experimental data performed into the system  
206 indicate that the liquid bulk alkalinity into the medium is never exhausted, preventing the loss of  
207 injected CO<sub>2</sub> used for pH control. On the contrary, the O<sub>2</sub> is produced during photosynthesis by  
208 microalgae and used by bacteria for their respiration, and it is partially removed from the culture  
209 broth due to mass transfer phenomena, mainly aeration into the sump installed on the reactor.

#### 210 ***Main changes implemented from ABACO model***

211 Despite the ABACO model served as the starting point for the development of ABACO-2, significant  
212 modifications have been implemented to enhance prediction accuracy and process understanding.  
213 Indeed, the ABACO model proposed by Sánchez-zurano et al., 2021, can be considered a  
214 preliminary study, conducted with a limited expertise regarding microalgae cultivation phenomena.  
215 Furthermore, this model was developed using a restricted dataset and calibrated using data from  
216 laboratory-scale experiments conducted under controlled conditions. In contrast, with ABACO-2, the  
217 intention is to calibrate parameters under industrial conditions, utilizing a more extensive dataset that  
218 encompasses diverse operational and climatic scenarios.

219

220

221 The foremost modification involved the integration of models to account for cell death and respiration,  
222 coupled with the variation in BSMO content within the culture, subsequently reduced by heterotrophic  
223 bacterial activity. This refinement also led to a reduction in the number of parameters necessitating  
224 calibration. As an additional parameter reduction strategy, it was assumed that phosphate  
225 consumption by bacteria is minimal and primarily relevant for microalgae. Consequently, phosphate  
226 consumption yields for these microorganisms were excluded from the calibration set. Regarding  
227 nutrient yields, equations were introduced to describe the dynamics of nutrient uptake by algae as a  
228 function of their concentration in the medium. In this context, process rates were adjusted to consider  
229 that  $\text{NO}_3$  consumption by algae is significant only when  $\text{NH}_4$  levels are substantially reduced.  
230 Furthermore, in relation to nutrients, a correction parameter was incorporated into the Monod  
231 equations to account for nutrient accumulation by microalgae, preventing zero growth in such  
232 scenarios. In the context of refining the calibration process, parameters associated with nutrient  
233 consumption by bacteria (originally calibrated) were set and adopted from the Activated Sludge  
234 Models (ASM), and an oxygen balance was introduced. The  $\text{O}_2$  concentration is a continuous  
235 measurement within the reactor and it significantly facilitated parameter recognition during the  
236 calibration process. Finally, the parameters of the cardinal temperature equations were adjusted  
237 using those proposed by Casagli et al., 2021, as they are more representative, having been  
238 calibrated while considering winter seasons.

### 239 **3.2. Model components**

240 This section summarizes the main model components:

- 241 •  $S_{\text{NH}_4}$  [ $\text{g}\cdot\text{m}^{-3}$ ]: ammonium. It is present in the influent, and it is consumed especially by microalgae  
242 and nitrifying bacteria and in a lower amount by heterotrophic bacteria.
- 243 •  $S_{\text{NO}_3}$  [ $\text{g}_{\text{NO}_3}\cdot\text{m}^{-3}$ ]: nitrate. This form of nitrogen is generally null in the influent, but it is generated by  
244 the nitrifying bacteria during the nitrification process. Nitrate is consumed by microalgae when  
245 ammonium concentration in the medium is low.

- 246 •  $S_{PO_4}$  [ $g_{PO_4} \cdot m^{-3}$ ]: phosphate. Phosphorus is present as a dissolved component in the water inlet.  
 247 Its consumption is mainly due to the activity of microalgae, while the uptake from bacteria is  
 248 considered negligible.
- 249 •  $S_{BSMO}$  [ $g_{BSMO} \cdot m^{-3}$ ]: biodegradable soluble organic matter. This is a fraction of the total COD,  
 250 assumed as 22%. It is consumed by heterotrophic bacteria and generated during the cellular  
 251 decay of both microalgae and bacteria.
- 252 •  $S_{O_2}$  [ $g_{O_2} \cdot m^{-3}$ ]: dissolved oxygen. Oxygen is produced by microalgae during photosynthesis and  
 253 consumed by microalgal respiration and by the activity of both bacterial populations. Moreover,  
 254 the dissolved oxygen can be stripped to the atmosphere by bubbling air into the reactor sump.
- 255 •  $X_{alg}$  [ $g_{alg} \cdot m^{-3}$ ]: microalgae biomass. Microalgae proliferate starting from an initial inoculum, thus  
 256 microalgae biomass is produced by fixing nitrogen and phosphorus, also consuming  $CO_2$  while  
 257 producing oxygen. Microalgae concentration in the inlet wastewater is considered negligible,  
 258 while a given amount is harvested every day. Moreover, their growth decreases due to cellular  
 259 death.
- 260 •  $X_{nit}$  [ $g_{nit} \cdot m^{-3}$ ]: nitrifying bacteria biomass. Nitrifying bacteria proliferate starting from an initial  
 261 inoculum by consuming nitrogen in the form of ammonium and releasing nitrate. It is assumed  
 262 that their concentration entering the system is negligible, while a given concentration is exiting  
 263 during the harvesting. Moreover, their growth decreases due to cellular death.
- 264 •  $X_{het}$  [ $g_{het} \cdot m^{-3}$ ]: heterotrophic bacteria biomass. Heterotrophic bacteria proliferate starting from an  
 265 initial inoculum by consuming the BSMO and nitrogen in the form of ammonium. It is assumed  
 266 that their concentration entering the system is negligible, while a given concentration is exiting  
 267 during the harvesting. Moreover, their growth decreases due to cellular death.

### 268 **3.3. Boundary conditions**

269 Concentrations must be always positive or equal to zero. This boundary condition can be expressed  
 270 as in equation (1): when a concentration is approaching zero (assuming  $\varepsilon$  in the order of  $10^{-8}$ ), its  
 271 derivative has to be equal or more than zero, meaning that it cannot generate negative matters.

272 
$$if \ X_i \leq \varepsilon \ \rightarrow \ \dot{X}_i|_{X_i=0} \geq 0 \quad (1)$$

273 As a result, all the balances implemented for this model have been implemented according to  
274 equation (2), guaranteeing the boundary conditions to be satisfied.

$$275 \quad \dot{X} = f(x, y) \cdot \frac{X}{X + \varepsilon} \quad (2)$$

### 276 **3.4. Biological processes**

277 Table 1 summarizes the processes taken into consideration of the microalgae and the bacterial  
278 growth, while **Error! Reference source not found.** is the relative matrix of the stoichiometric  
279 parameters. The mass balances for the microorganism's growth have been built according to  
280 equation (3):

$$281 \quad \text{Inlet} - \text{Outlet} + \text{Reaction} = \text{Accumulation} \quad (3)$$

282 where the *Inlet* and *Outlet* are the flowrates in [ $\text{m}^3 \cdot \text{s}^{-1}$ ] in and out of the system, generically defined  
283 as (4) and (5):

$$284 \quad \text{Inlet} = Q_d X_{in} \quad (4)$$

$$285 \quad \text{Outlet} = Q_h X_{out} \quad (5)$$

286 where  $Q_d$  is the dilution flow rate in [ $\text{m}^3 \cdot \text{s}^{-1}$ ],  $Q_h$  is the harvesting flow rate in [ $\text{m}^3 \cdot \text{s}^{-1}$ ],  $X_{in}/ X_{out}$  (or  $S_i/$   
287  $S_{out}$ ) is the concentration of component inlet or outlet in [ $\text{g} \cdot \text{m}^{-3}$ ].

288 The reaction ( $r_i$ , [ $\text{g} \cdot \text{m}^{-3} \cdot \text{day}^{-1}$ ]) term can be obtained by summing the product of the stoichiometric  
289 coefficients,  $\nu_{i,j}$  (Table 3) and the process rate,  $\rho_j$ , as described in (6) (Henze et al., 2000)

$$290 \quad r_i = \sum_j \nu_{i,j} \rho_j \quad (6)$$

291 In summary, the processes considered in the ABACO-2 model are:

- 292 •  $\rho_1$ : microalgae growth in  $\text{NH}_4^\pm$ . Microalgae grow photosynthetically using  $\text{NH}_4^+$  as a nutrient  
293 source, and contemporarily consuming  $\text{PO}_4^{3+}$  and  $\text{CO}_2$  while producing  $\text{O}_2$ .

- 294 •  $\rho_2$ : microalgae growth in  $\text{NO}_3^-$ . Microalgae grow photosynthetically using  $\text{NO}_3^-$  as a nutrient  
295 source, and contemporarily consuming  $\text{PO}_4^{3+}$  and  $\text{CO}_2$  while producing  $\text{O}_2$ . The growth in this  
296 nitrogen source is activated only once the medium is decreasing in  $\text{NH}_4^+$  concentration.
- 297 •  $\rho_3$ : microalgae decay. This process includes both the algal biomass loss (decay), increasing the  
298 BSMO concentration in the medium, and the algal respiration that leads to a consumption of  
299 oxygen all over the entire process.
- 300 •  $\rho_4$ : nitrifying bacteria growth. Nitrifying bacteria growth consumes  $\text{NH}_4^+$  and  $\text{O}_2$  and produces  
301  $\text{NO}_3^-$ .
- 302 •  $\rho_5$ : nitrifying bacteria decay. Bacterial biomass loss due to their decay; it leads to an increase in  
303 the BSMO concentration.
- 304 •  $\rho_6$ : heterotrophic bacteria growth. Heterotrophic bacteria growth consuming the BSMO,  $\text{O}_2$  and  
305  $\text{NH}_4^+$ .
- 306 •  $\rho_7$ : heterotrophic decay. Bacterial biomass loss due to their decay (it leads to an increase in the  
307 BSMO concentration).

#### 308 **3.4.1. Photosynthesis and respiration**

309 The growth rate as a function of light was modelled using the equation proposed by Molina (Grima  
310 et al., 1994), as described in equation (7), where  $I_k$  in [ $\mu\text{E}\cdot\text{m}^{-2}\cdot\text{s}^{-1}$ ] is the irradiance constant that  
311 represents the equivalent irradiance necessary to reach half of the maximal growth rate,  $n$  is the  
312 shape constant and  $I_{av}$  is the average light inside the reactor in [ $\mu\text{E}\cdot\text{m}^{-2}\cdot\text{s}^{-1}$ ].

$$313 \quad \mu(I_{av}) = \frac{I_{av}^n}{I_k^n + I_{av}^n} \quad (7)$$

314 The average light inside the culture was expressed following equation (8), and it depends on the  
315 incident light  $I_0$  [ $\mu\text{E}\cdot\text{m}^{-2}\cdot\text{s}^{-1}$ ], the extinction coefficient  $K_a$  [ $\text{m}^2\cdot\text{g}^{-1}$ ], the algal biomass concentration  
316 ( $X_{alg}$ ) in [ $\text{g}\cdot\text{m}^{-3}$ ] and the culture depth  $h$  [m].

$$317 \quad I_{av} = \frac{I_0}{K_a X_{alg} h} (1 - \exp(-K_a X_{alg} h)) \quad (8)$$

318 Moreover, the average light was used to express the microalgal endogenous respiration as given by  
319 equation (9); where  $m_{max}$  and  $m_{min}$  are the maximum and the minimum respiration in [ $\text{day}^{-1}$ ],  $I_{kr}$  is the  
320 irradiance necessary to stop photosynthesis and let begin the respiration and  $n_r$  is the shape form  
321 for respiration.

$$322 \quad m_{alg} = m_{min} + \frac{m_{max} I_{av}^{n_r}}{I_{kr}^{n_r} + I_{av}^{n_r}} \quad (9)$$

323 Finally, bacterial decay has been taken into consideration as a constant effect during the cultivation  
324 process.  $m_{nit}$  and  $m_{het}$  [ $\text{day}^{-1}$ ] have been modelled as a percentage of the maximum growth rate (as  
325 summarized in Table 4) corrected by a coefficient dependent on the temperature  $\theta$ , as described in  
326 equation (10).

$$327 \quad \theta = \theta_i(T - 20^\circ\text{C}) \quad (10)$$

328 Where  $\theta_i$  are specific parameters that depend on the bacterial population considered (Table 3).

### 329 **3.4.2. Influence of pH, temperature, dissolved oxygen and nutrients**

330 As described in Table 1, for each microorganism, the growth rate depends on a maximum specific  
331 growth rate  $\mu$  value multiplied by a series of normalized factors that depends on the culture conditions  
332 of temperature, pH,  $\text{O}_2$  and nutrient concentration. The growth rates of microalgae exhibit a bell-  
333 shaped function in response to temperature and pH. Initially, as temperature (or pH) increases from  
334 low values, the growth rate rapidly increases until it reaches its maximum, corresponding to the  
335 optimal parameter value. However, beyond the optimum, the growth rate decreases sharply with  
336 further increases in temperature (or pH). The minimum, maximum, and optimal values of these  
337 parameters can be determined through laboratory measurements using the photo-respirometric  
338 method, and the summarized values are in Table 4. It is possible to observe that bacteria parameters  
339 differ from one of the microalgae since their growth is favoured by higher values of both temperature  
340 and pH. The growth dependence can be described through a cardinal equation with inflexion,  
341 developed for the first time by Bernard et al. (Bernard and Rémond, 2012) (11). Similarly, the model  
342 proposed by Ippoliti et al. was used to describe the pH dependence (Ippoliti et al., 2016) (12).

343 
$$\overline{\mu(T)} = \frac{(T - T_{max})(T - T_{min})^2}{(T_{opt} - T_{min})[(T_{opt} - T_{min})(T - T_{opt}) - (T_{opt} - T_{max})(T_{opt} + T_{min} - 2T)]} \quad (11)$$

344 
$$\overline{\mu(pH)} = \frac{(pH - pH_{min})(pH - pH_{max})^2}{(pH_{opt} - pH_{min})[(pH_{opt} - pH_{min})(pH - pH_{opt}) - (pH_{opt} - pH_{max})(pH_{opt} + pH_{min} - 2pH)]} \quad (12)$$

345 Regarding the effect of dissolved oxygen, it is known that high concentrations are inhibitory for  
 346 microalgal photosynthesis. According to previous studies on *Scenedemesus sp.*, the growth rate can  
 347 be reduced by 25% when the concentration is increased up to 150% Sat, while below 250% Sat the  
 348 photosynthesis is completely stopped. This effect was modelled using the equation proposed by  
 349 Costache et al., 2013 and reported in equation (13). On the contrary, oxygen has been modelled as  
 350 a nutrient source for bacteria growth, as described below.

351 
$$\overline{\mu(O_2)_{alg}} = 1 - \left( \frac{S_{O_2}}{S_{O_2,max}} \right)^z \quad (13)$$

352 Finally, the influence of nutrient concentration on the growth rate was taken into account. As  
 353 mentioned, nitrogen is a fundamental macronutrient that must be provided to microalgae to ensure  
 354 their growth. The inorganic nitrogen can be assimilated into acids for the protein formations in many  
 355 forms, such as  $NH_4^+$ ,  $NO_2^-$  and  $NO_3^-$ . However, in this study, the main nitrogen form present in  
 356 wastewater was ammonium, while nitrate was formed only after the complete nitrification process.  
 357 Ammonium is the favoured nitrogen form for microalgae as it requires less energy to be assimilated.  
 358 Only after a given concentration threshold do microalgae begin to consume  $NO_3^-$ , which will be  
 359 transformed into  $NH_4^+$  to be assimilated into the cells. Phosphate is another fundamental  
 360 macronutrient for microalgal growth, as it is necessary for the synthesis of RNA into the nucleotides,  
 361 while it is assumed that this component is not consumed by bacteria. The growth rate as a function  
 362 of the substrate concentration, has been modelled using the Monod equation, as described in (14),  
 363 (Monod, 1949)

364 
$$\overline{\mu(S_i)} = \frac{S_i}{S_i + K_s} \quad (14)$$

365 The Monod equations for the nitrogen and the phosphorus for the process n.1 and 2 in **Error!**  
 366 **Reference source not found.** have been modified by the inclusion of a correction factor. With this



367 modification, zero-growth when no longer nitrogen/phosphate are present in the medium was  
368 avoided. Indeed, it is already known that microalgae can store nutrients in cells guaranteeing their  
369 survival and growth even when the medium is limited in nutrients. This fact can be represented by  
370 more complex models such as the Droop model (Droop, 1970), which considers the cells quota of  
371 the limiting element. However, quotas are difficult to be estimated as they required specific laboratory  
372 techniques. For this reason, in this work, a simplified description of this phenomenon was chosen by  
373 correcting the concentrations in the Monod equation as the sum of the component available in the  
374 medium and the one present in the algal biomass (equal to 10% in nitrogen and 2% in phosphorus,  
375 multiplied by the “assimilation” factor  $\alpha$ ) (14), (15).

$$376 \quad S_N = S_{N,medium} + X_{alg} * 0.1 * \alpha \quad (15)$$

$$377 \quad S_P = S_{P,medium} + X_{alg} * 0.02 * \alpha \quad (16)$$

378 The kinetic parameters used for the Monod equation are summarized in Table 3.

### 379 **3.4.3. Nutrient yields**

380 Nutrient yield can be defined as the amount of nutrients consumed from the medium per gram of  
381 biomass produced. In the literature, it can be found that the nutrient yield for algae is not constant,  
382 but changes depending on the nutrient amount present in the medium. More specifically, it was found  
383 that the nutrient uptake rate is higher at lower nutrient concentrations until it is reached a maximum.  
384 This can be explained by some biological mechanisms like the “luxury uptake” (Solovchenko et al.,  
385 2019): microalgae store a larger amount of nutrients than the ones necessary for immediate growth.  
386 It is possible to suppose that nutrients yield not only depends on the nutrient concentrations in the  
387 medium but even on environmental conditions and process parameters. However, modelling this  
388 phenomenon is complex, and in the literature can be found different results that mainly depend on  
389 the strain used and the type of experiment performed. The equations developed by Zurano et al.,  
390 2021 were taken as a good approximation of ammonium and phosphorus consumption rates by  
391 microalgae, as described in equation (17), where S is the substrate consumed by microalgae ( $\text{NH}_4^+$ ,  
392  $\text{NO}_3^-$  or  $\text{PO}_4^{3-}$ ). It is possible to observe that the equations are the combination of a Monod equation

393 together with a Cardinal limited by a maximum value; the equation parameters are summarized in  
 394 Table 5.

$$395 \quad Y_{s,alg} = \left[ \frac{Y_{max} S^{ts}}{S_N^{ts} K_{s,Y_s}^{ts}} \right] + \left[ \frac{(S - S_{max})(S - S_{min})^2}{(S_{opt} - S_{min}) \left( ((S_{opt} - S_{min})(S_N - S_{opt})) - ((S_{opt} - S_{max})(S_{opt} + S_{min} - 2S)) \right)} \right] \quad (17)$$

396 Regarding the nutrient yield of bacteria, the ones proposed by the ASM models (Henze et al.,  
 397 2000) were considered a good approximation, and they are summarized in Table 3.

### 398 **3.4.4. Dissolved oxygen**

399 During the day, microalgae produce oxygen through photosynthesis, which is partially consumed for  
 400 algal and bacteria respiration. At the same time, dissolved oxygen can be desorbed to the  
 401 atmosphere according to two different phenomena: (i) natural mass transfer from the culture to the  
 402 atmosphere in the reactor channels and paddlewheel; (ii) oxygen release and consecutive reduction  
 403 of the culture dissolved oxygen thanks to the bubbling of air in the reactor sump. The two phenomena  
 404 are represented by two different mass transfer coefficients  $K_{la}$  (equal to 1.0 and 110 h<sup>-1</sup> respectively)  
 405 and Henry law as described in (18):

$$406 \quad m_{O_2} = K_{la_i}(H_{O_2}P_{O_2} - S_{O_2}) \quad (18)$$

## 407 **4. Model parameters**

### 408 **4.1. Calibration procedure**

409 Figure 2 represents the calibration strategy adopted. The experimental dataset used to calibrate the  
 410 model parameters was selected to include data from different seasons, such as summer, winter, and  
 411 intermediate seasons (28/04-15/05, 9/08-15/08, 1/11-15/11). In total, the calibration days chosen  
 412 were 41 (20% of the total amount of data). In this way, it was possible to address the parameters by  
 413 accounting for various climatic conditions. The final set of parameters was chosen once the objective  
 414 function described in (19) was minimized.

$$415 \quad Obj = \sum \frac{\sum (y_{sim} - y_{exp})^2}{\sigma_{exp}} \quad (19)$$

416 where  $y_{sim}$  is the model output,  $y_{exp}$  the experimental data and  $\sigma_{exp}$  is the experimental data standard  
417 deviation. The experimental data used for the model calibration regarded  $X_{tot}$ ,  $S_{NH_4}$ ,  $S_{PO_4}$ ,  $S_{NO_3}$ ,  $S_{BSMO}$ ,  
418  $S_{O_2}$  where  $X_{tot}$  was defined as the sum of  $X_{alg}$ ,  $X_{nit}$  and  $X_{het}$  and evaluated experimentally as the total  
419 dry weight. The model calibration was carried out using Scipy library in Python and “Nelder-Mead”  
420 algorithm which is a robust algorithm mainly used for solving unconstrained optimization problems  
421 (Gao and Han, 2012). The list of calibrated parameters with their corresponding values is presented  
422 in

423 Table 6.

## 424 **4.2. Sensitivity analysis**

425 Table 7 presents the findings of a sensitivity analysis that examined all biological and process  
426 parameters together with the associated standard deviation. In this analysis, each parameter was  
427 individually varied by +/-20% from its nominal value, and the percentage error (20) between the  
428 nominal parameter value ( $y_{nom}$ ) and the varied parameter value ( $y_{var}$ ) was evaluated.

$$429 \quad \% \text{ err} = \frac{\sum |y_{nom} - y_{var}|}{\sum y_{var}} * 100 \quad (20)$$

430 Results indicate that the most sensible parameters are the ones for microalgae growth rate as a  
431 function of light ( $I_{av}$ ,  $K_a$ ,  $n$ ), the maximum growth rates of all the organisms ( $\mu_{max,alg}$ ,  $\mu_{max,nit}$ ,  $\mu_{max,het}$ )  
432 and the nutrient yield of  $NH_4^+$  and  $NO_3^-$  ( $Y_{NH_4,alg}$ ,  $Y_{NO_3,nit}$ ,  $Y_{NH_4,nit}$ ). Additionally, the cardinal parameters  
433 ( $T_{max}$ ,  $T_{min}$ ,  $T_{opt}$ ) of temperature and pH ( $pH_{max}$ ,  $pH_{min}$ ,  $pH_{opt}$ ) show to be highly sensitive. Given their  
434 significant impact on the final prediction, these parameters should be carefully selected based on  
435 the biological system analysed and the climatic conditions. Notably, only a few of the nutrient yields  
436 were deemed relevant to model error.

## 437 **4.3. Parameters uncertainty and error propagation**

438 Once the most sensible parameters have been identified, it was possible to calculate the model  
439 variance and the confidence interval (Denis Dochain, 2001). From the sensitivity analysis, it was

440 possible to define a sensitivity matrix as (21), which collects the functions of the given output  $y$  by  
 441 varying the parameter  $p_j$ .

$$442 \quad S = \left[ \frac{\delta y}{\delta p_1} ; \frac{\delta y}{\delta p_2} ; \dots ; \frac{\delta y}{\delta p_j} \right] \quad (21)$$

443 The standard deviation of the parameter can be calculated as (22), where  $C_{jj}$  is the covariance matrix  
 444 and  $p_j$  is the associated parameter:

$$445 \quad \vartheta_j^2 = p_j \sqrt{C_{j,j}} \quad (22)$$

446 The covariance matrix is the inverse of the Fisher information matrix (23), defined as the variance of  
 447 the score function (Fujita et al., n.d.).

$$448 \quad F = C^{-1} \quad (23)$$

449 And it can be calculated starting from the sensitivity analysis according to (24):

$$450 \quad F = S^T Q^{-1} S \quad (24)$$

451 where  $Q$  is the array of the measured standard deviation.

452 Once the covariance of the parameter has been evaluated, it was possible to estimate the model  
 453 error propagation of the output variable  $y$  at the given instant time  $t$  as (25):

$$454 \quad \sigma_y(t) = \sqrt{\sum_{i=1}^m S_i(t)^2 \vartheta_{p_j}^2} \quad (25)$$

455 The model confidence interval at 95% has been calculated on the model output as (26):

$$456 \quad [y_i - 1.95\sigma_y ; y_i + 1.95\sigma_y] \quad (26)$$

## 457 **5. Model validation**

458 The model prediction accuracy has been evaluated by calculating the normalized squared root error  
 459 (NRMSE) and Theil's inequality coefficient (TIC) (H. Theil. et al., 1959), as described in (26), (27).

460 Results are reported in Table 8, it is important to note that when the TIC is lower than 0.3, it is

461 possible to consider a good agreement between the experimental data and the model predictions.  
462 Additionally, Figure 3 to Figure 5 represent the model estimation and the respective experimental  
463 data, as described in the next session.

$$464 \quad NRMSE = \frac{\sqrt{\sum (y_{sim} - y_{exp})^2}}{(y_{exp,max} - y_{exp,min})} \quad (26)$$

$$465 \quad TIC = \frac{\sqrt{\sum (y_{sim} - y_{exp})^2}}{\sum y_{sim}^2 + \sum y_{exp}^2} \quad (27)$$

466 Overall, it is possible to affirm that the model can accurately reproduce the biological system. The  
467 ABACO-2 model is remarkably accurate for describing the total biomass concentration and the  
468 nutrient concentration evolution (NRMSE between 0.14 and 0.23, TIC between 0.16 and 0.24).  
469 Additionally, the model accurately can trace the dissolved oxygen in the culture (NRMSE= 0.14,  
470 TIC=0.21).

## 471 **6. Discussion**

### 472 **6.1. Simulation results**

473 Although microalgae-bacteria consortia are considered a promising technology for wastewater  
474 treatment, they still address several challenges. An accurate microalgae-bacteria model is a powerful  
475 tool to overcome the bottlenecks of this technology (Aparicio et al., 2023). The ABACO-2 model aims  
476 to act as a tool for robust and accurate prediction of the evolution of biomass concentration in a  
477 microalgae-bacteria system, and, therefore, to differentiate between the evolution of both  
478 populations in the face of operational and environmental conditions. Figure 3A represents the  
479 evolution of the total biomass concentration from 15<sup>th</sup> May to 15<sup>th</sup> November. The dots represent the  
480 experimental data while the model is shown with a solid line, and the shading is the model confidence  
481 interval at 95%. Total biomass is mean the sum of the contributions of algae and bacteria that can  
482 be approximated to the biomass experimentally evaluated through the dry weight method. The  
483 results showed that the model reproduces the trend of the experimental data, with a NRMSE=0.21  
484 and TIC=0.16 (Table 8). The concentration of heterotrophic and nitrifying bacteria over the study

485 period is shown in Figure 3B. According to the simulations, heterotrophic bacteria exhibit higher  
486 concentrations than nitrifying bacteria as they vary between 0 and  $80 \text{ g}_{\text{net}} \cdot \text{m}^{-3}$ , whereas nitrifying  
487 bacteria range from 0 to  $10 \text{ g}_{\text{nit}} \cdot \text{m}^{-3}$ . Regarding heterotrophic bacteria, the strong fluctuations  
488 observed could be explained by the large variability in the COD concentration in the influent ( $100 -$   
489  $600 \text{ gO}_2 \cdot \text{m}^{-3}$ ). This variability arises from the use of two different types of water sources, one from  
490 the University and the other from the city, with the latter typically containing a higher organic matter  
491 content. The concentration over the months of the nitrifying bacteria was lower, considering their  
492 slower maximum growth rate compared to the one of heterotrophic bacteria. Results show that the  
493 concentration of nitrifying bacteria increased from October to November. This increase may be due  
494 to a reduction in the aeration rate in this specific period, which decreased from  $200 \text{ L} \cdot \text{min}^{-1}$  (set-point  
495 in normal operations) to  $50 \text{ L} \cdot \text{min}^{-1}$ . During that months, the dissolved oxygen concentration  
496 increased in the culture, as the aeration was insufficient to remove it efficiently. Previous studies  
497 have shown that dissolved oxygen concentration strongly influences the growth of microalgae, as it  
498 has an inhibitory effect on photosynthetic activity (Rossi et al., 2020a). Thus, by decreasing the  
499 concentration of microalgae, nitrifying activity is favoured, as both populations compete for the  $\text{N-}$   
500  $\text{NH}_4^+$  present in the medium. Previous authors suggested that competition for  $\text{N-NH}_4^+$  is the most  
501 frequently negative interaction between microalgae and AOB (Aparicio et al., 2022b). The microalgal  
502 biomass concentration is represented in Figure 3C. Algal productivity is primarily influenced by  
503 variations in light and temperature throughout the seasons (Muñoz and Bernard, 2021). During  
504 spring, the biomass concentration is approximately  $0.7 \text{ g}_{\text{alg}} \cdot \text{L}^{-1}$ , while in summer it can reach higher  
505 values of up to  $1.5 \text{ g}_{\text{alg}} \cdot \text{L}^{-1}$ . However, during the colder seasons, it decreases to  $0.3 \text{ g}_{\text{alg}} \cdot \text{L}^{-1}$ . Overall,  
506 the model effectively captures the evolution of biomass concentration, highlighting the prevalence of  
507 algae biomass compared to bacterial biomass within the culture. Although there is a lack of  
508 experimental data on bacterial concentration, this outcome remains reasonable, supported by  
509 analysis conducted in previous studies on similar systems (Sánchez Zurano et al., 2020).

510 Figure 4 represents the  $\text{PO}_4^{3-}$ ,  $\text{NO}_3^-$ ,  $\text{NH}_4^+$  and BSMO concentration in  $\text{g} \cdot \text{m}^{-3}$  respectively. In Figure  
511 4A it is shown that the phosphate concentration in the culture can vary between 10 and  $60 \text{ g}_{\text{PO}_4} \cdot \text{m}^{-3}$ .  
512 The uptake of this component depends only on the activity of microalgae, given that the influence of

513 bacteria can be considered negligible. In previous studies, it has been demonstrated that the  
514 consumption of phosphate is efficient, but not sufficient to lower it to a concentration below the  
515 minimum required for the waster discharge (Nordio et al., 2023). Figure 4B represents the  $\text{NO}_3^-$   
516 concentration, that remained constant from May to October, however, from October to November, it  
517 was observed an increase in the  $\text{NO}_3^-$  concentration, mainly generated during the nitrification process  
518 by nitrifiers. The concentration of this compound can vary greatly (between 0 and  $300 \text{ g}_{\text{NO}_3} \cdot \text{m}^{-3}$ )  
519 depending on the activity of the nitrifying bacteria, which, as already explained, was enhanced at the  
520 end of the study. Nitrate increase and accumulation in the system can be considered one of the main  
521 challenges in microalgae-bacteria-based systems. A decrease in microalgae activity leads to an  
522 increase in nitrifying activity, which results in the accumulation of nitrate in the medium. The nitrate  
523 generated must be consumed by the microalgae. However, as long as ammonium is available in the  
524 medium, it will not be consumed or will be consumed slowly, in breach of discharge regulations.  
525 Therefore, ensuring correct microalgae activity is essential to achieve treated water at the end of the  
526 process. Regarding the organic matter, its degradation is due to the activity of the heterotrophic  
527 bacteria and it can be present with a concentration of up to  $250 \text{ g}_{\text{O}_2} \cdot \text{m}^{-3}$  in the culture (Figure 4C).  
528 Finally, in Figure 4D there is the evolution of the ammonium concentration. It is possible to observe  
529 that, despite the high  $\text{NH}_4^+$  concentration entering the system with the wastewater, in the outlet its  
530 concentration is mostly lower than  $60 \text{ g}_{\text{NH}_4} \cdot \text{m}^{-3}$ , meaning that microalgae and nitrifiers can uptake  
531 this nutrient with a high efficiency. The peak generated by the simulation is mainly due to the high  
532 concentration of this compound entering the system during the dilution/harvesting process at a  
533 specific time of the day.

534 Concluding, Figure 5 represents the simulation of the dissolved oxygen in the culture. Specifically,  
535 Figure 5A shows the experimental and simulated values of dissolved oxygen concentration along  
536 the entire study period, while Figure 5B shows the representation of the dissolved oxygen  
537 concentration in a shorter period. The concentration of dissolved oxygen can reach a high  
538 concentration during the day due to the microalgal photosynthesis (up to  $25 \text{ mg}_{\text{O}_2} \cdot \text{L}^{-1}$ ), while it  
539 decreases to anoxic conditions during the night due to the couple effect the algae and bacteria  
540 respiration.

541 The results obtained show that the evolution of nutrients in the system together with the simulated  
542 biomass concentration agree with those obtained in the experimental data, demonstrating the  
543 usefulness of ABACO-2 in microalgae-based systems for wastewater treatment, and its potential on  
544 an industrial scale.

## 545 **6.2. Case study: evaluating microalgae-bacteria consortia as function of the operational** 546 **conditions**

547 Studying the populations living in wastewater systems treated with microalgae poses a significant  
548 challenge, primarily because there are no fully validated protocols to effectively differentiate between  
549 bacterial and microalgal communities. The primary method for assessing biomass in raceway  
550 reactors is dry weight, encompassing contributions from both algae and bacteria. Separating them  
551 remains challenging yet significant, as their ratios impact various process outcomes, such as  
552 biomass quality and water remediation efficiency. Some methods, like successive filtrations based  
553 on cell size differences, have been explored, though they often result in a notable presence of  
554 bacteria clinging to microalgae due to cell aggregation (Sánchez-Zurano et al., 2020). Alternative  
555 methods, including flow cytometry techniques (FCM), prove valuable in assessing the relative  
556 composition of mixed microorganism populations, encompassing both prokaryotes and eukaryotes.  
557 This approach discriminates between groups by analyzing intrinsic characteristics of individual cells,  
558 such as size, complexity, and autofluorescence. Additionally, molecular identification techniques like  
559 amplification of 16S and 18S rDNA sequences serve to evaluate microbial community structure  
560 (Barreiro-Vescovo et al., 2021). Alongside these methods, photo-respirometry, based on traditional  
561 respirometry, has been employed to discern population differences (Rossi et al., 2018). However,  
562 these methods lack a direct correlation in biomass concentration ( $\text{g}\cdot\text{L}^{-1}$ ), which is more  
563 straightforward to interpret.

564 In this context, mathematical models offer a useful tool of indirectly study how the balance between  
565 populations evolves. Operational conditions, notably cultivation height, dilution/harvesting strategy,  
566 and oxygen removal capacity, exhibit a substantial influence. This section presents a case study  
567 employing the ABACO-2 model to assess how the proportion between algae and bacteria shifts



568 based on the operational conditions. Simulations have been carried out using the same solar  
569 radiation and temperature registered for the validation of the model. On the contrary, the inlet values  
570 of nutrient concentration have been maintained constant (as a average values measured in the  
571 wastewater medium) in order to avoid their influence in the evaluation of the process conditions (180  
572  $\text{mg}\cdot\text{L}^{-1}$   $\text{NH}_4^+$ , 30  $\text{mg}\cdot\text{L}^{-1}$   $\text{PO}_4^{3-}$ , 80  $\text{mg}\cdot\text{L}^{-1}$  BSMO, 3.4  $\text{mg}\cdot\text{L}^{-1}$   $\text{NO}_3^-$ ).

### 573 ***Culture height***

574 The cultivation height is one of the fundamental parameters to consider when operating raceway-  
575 type reactors as it significantly influences the penetrative capacity of light within the cultivation. It has  
576 been demonstrated that light reaches the cells only in the first three centimeters of culture, while the  
577 rest remains in a state of darkness due to an effect of autoshading, and, therefore, photosynthetically  
578 inactive. Furthermore, light penetration depends on other factors, such as the extinction coefficient  
579 ( $K_a$ ), which can vary from cultivation to cultivation and depends on the property of microalgae to  
580 scatter the received light (Barceló-Villalobos et al., 2019).

581 In general, facilities that aim to treat large quantities of water prefer to operate at a rather high culture  
582 height, around 30 cm. However, this could be a disadvantage in terms of producing high-quality  
583 biomass, as the dark zone favors the growth of bacterial populations over phototrophic ones. Figure  
584 6 A,B and C show the populations varying with cultivation height among the seasons (summer,  
585 spring and autumn). As expected, at 8 cm, the algal productivity is favored at the expense of the  
586 amount of treated water, with the maximum concentration reached in spring as it is the period when  
587 the maximum irradiance is reached (Figure 6A). The possibility of being able to increase productivity  
588 by reducing the culture height has already been studied through the development of new reactors  
589 called "thin layers" that operate at around 2 cm; they have also been tested for treating wastewater  
590 in previous studies (Morillas-España et al., 2021a). On the contrary, microalgal concentration  
591 decreases as much as the culture height increases, mitigating the effects related to the different  
592 seasons, in favour of the proliferation of the bacterial population (Figure 6B,C). This is particularly  
593 evident in the case of nitrifiers. An increased water depth and greater availability of ammonium,  
594 owing to a reduced uptake capacity by microalgae, enable an increase in their activity. Previous

595 works demonstrated that the depth of the culture has a striking effect on the composition of the  
596 microalgae-bacteria consortia, specially in relative abundance of nitrifiers (Figure 6C). Remarkably,  
597 at an 8 cm depth where algae activity is more significant, ammonium consumption mainly occurs  
598 within the algae population, resulting in minimal involvement of nitrifying bacteria. Conversely,  
599 variations in cultivation height appear to have little effect on the concentration of heterotrophic  
600 bacteria (Figure 6B). This is because they do not compete with microalgae for nutrient uptake like  
601 nitrifying bacteria; their primary substrate is organic carbon.

602 In conclusion, the choice of the optimal culture height is of relevance and its regulation mainly depend  
603 on the specific goals of the remediation process. These goals may involve achieving high-quality,  
604 productive biomass or ensuring efficient water treatment on a larger scale. While a lower culture  
605 height is generally recommended to facilitate light penetration, further studies should be carried to  
606 avoid heat accumulation and the cellular death. Moreover, it's essential to recognize that significantly  
607 increasing the culture depth could enhance the activity of nitrifying bacteria and lead to the  
608 accumulation of  $\text{NO}_3^-$  within the reactor. Based on the outcomes of this simulation study, a culture  
609 height of 15 cm appears as a good compromise between treated water quantity, productivity, and  
610 balance between algal and bacterial populations.

### 611 ***Dilution/harvesting rate***

612 The harvesting/dilution factor plays a crucial role in microalgae industrial production. When deciding  
613 on the best approach to adopt, key considerations include the optimal dilution rate and its application  
614 method - whether through continuous or semi-continuous mode. In the first case, dilution occurs  
615 gradually over the 12 hours of daylight, while in the latter, both dilution and harvesting take place at  
616 specific moments of the day. Figure 6 D, E and F illustrate how varying the dilution rate can impact  
617 the productivity and composition of algal-bacterial populations, assuming to operate the reactor in a  
618 semi-continuous mode. The optimal dilution rates for algae range between 0.15 to 0.2  $\text{day}^{-1}$ ,  
619 exceeding these rates leads to a significant decrease in productivity (Figure 6D). This finding is  
620 consistent with previous research in similar raceway reactors, which suggested a fixed optimal  
621 dilution rate of 0.2  $\text{day}^{-1}$  throughout the year (Morillas-España et al., 2020). Concerning the bacterial

622 population, it is evident that nitrifying activity decreases significantly beyond a dilution rate of 0.2 day<sup>-1</sup>. This phenomenon, known as "culture washout," indicates that the growth rate of nitrifying bacteria  
623 lags behind the dilution rate, potentially affecting process effectiveness (Figure 6F). Conversely, a  
624 contrasting positive impact is observed on heterotrophic bacteria with increased dilution rates (Figure  
625 6E). This could be attributed to their rapid growth rate and the enhanced organic matter influx,  
626 promoting proliferation.

628 In summary, the simulations presented in this study underscore the critical importance of selecting  
629 the optimal dilution factor for the efficient operation of raceway reactors. Traditionally, dilution factors  
630 are determined experimentally through batches, which establish the maximum growth rate and  
631 consequently the dilution rate. Alternatively, some studies have suggested comparing reactors at  
632 different dilutions operated in parallel. While these methods are effective, they can be laborious and  
633 time-consuming. Furthermore, conventional laboratory techniques primarily evaluate productivity in  
634 terms of dry weight without delving into the dynamics of the populations involved. Therefore, our  
635 research demonstrates that a simulation-based approach offers a viable alternative for identifying  
636 the most effective dilution and harvesting strategies.

### 637 ***Air desorption***

638 The concentration of oxygen in a microalgae culture is crucial in biological systems. When oxygen  
639 levels surpass air saturation, they can induce inhibitory effects due to the diffusion of dissolved  
640 oxygen through microalgae membranes, resulting in oxidative stress on the cells. This inhibitory  
641 impact becomes more pronounced with prolonged exposure to elevated oxygen levels (Antonino  
642 Baez and Joseph Shiloach, 2014). Microalgae, as photosynthetic organisms, generate oxygen while  
643 consuming carbon dioxide, leading to its accumulation in the culture. Studies, such as the one  
644 conducted by Rossi et al. in 2020, have shown that excessive oxygen accumulation in cultures can  
645 hinder microalgal cell growth (Rossi et al., 2020b). However, there is a scarcity of research assessing  
646 how oxygen levels actually influence productivity on a large scale. The prevailing assumption is that  
647 oxygen is naturally removed through channels or within the paddlewheel zone. Nonetheless, our

648 experimental data presented herein emphasize the necessity of air injection to reduce oxygen levels  
649 in the reactor.

650 Figure 6G, H, and I illustrate the simulation results in scenarios both without air injection and with a  
651  $K_{La}$  equal to  $110 \text{ h}^{-1}$ . Once again, it is evident that forced air input is advantageous in promoting algal  
652 population production compared to bacterial populations (Figure 6G). Specifically, when air is not  
653 removed, microalgal concentration drastically decreases by 65%, underscoring the significance of  
654 air injection in the reactor to lower dissolved oxygen levels. Concerning the bacteria, it's notable that  
655 air injection predominantly affects nitrifying population, with heterotrophic ones being less affected.  
656 Heterotrophic bacteria exhibit a slight decrease in concentration when air isn't injected. Conversely,  
657 nitrifying bacteria show significant growth when oxygen isn't removed from the reactor using  
658 compressed air. These results align with the model validation discussed earlier and may offer an  
659 explanation for occasional  $\text{NO}_3^-$  accumulations in cultures. As previously explained, validation data  
660 indicated increased nitrification activity when air injection was reduced from  $200 \text{ L min}^{-1}$  to  $50 \text{ L min}^{-1}$ ,  
661  $^1$ , unfavoring algal growth but favoring nitrification. These simulations confirm this trend, although  
662 further experimental studies are needed for confirmation.

663 In conclusion, these simulations reaffirm the critical significance of oxygen removal from the reactor,  
664 not only for enhancing productivity but also for ensuring effective water remediation.

## 665 **Conclusions**

666 ABACO-2 is a comprehensive model for microalgae-bacteria consortia in wastewater systems. The  
667 model was calibrated and validated in a pilot-scale wastewater treatment reactor, exposed to  
668 environmental changes and fed with real urban wastewater (with daily changes in the concentration  
669 of nitrogen, phosphorus and organic matter), over a long period (May-November). The model  
670 allowed to predict the biomass, dissolved oxygen and nutrient concentration evolution with high  
671 accuracy. Overall, the use of the ABACO-2 model's relative simplicity allows for good predictions  
672 while offering advantages in terms of understanding, practicality, efficiency, and versatility.  
673 Concluding, the ABACO-2 model can be considered a useful biological model for the description of  
674 algae-bacteria in wastewater systems. In order to increase the robustness, in the future it will be

675 necessary to carry out additional validation studies in several data set (accounting for different  
676 climatologies and wastewater types) and in higher industrial scales.

#### 677 **Credit authorship contribution statement**

678 **R. Nordio:** Investigation, Formal Analysis, Validation, Software, Data Curation, Visualization, Writing  
679 – Original Draft; **E. Rodríguez-Miranda:** Investigation, Formal Analysis, Validation, Software, Data  
680 Curation, Writing – Original Draft; **F. Casagli:** Formal analysis, Validation; **A. Sanchez-Zurano:**  
681 Investigation, Writing – Original Draft; **J. L. Guzmán:** Conceptualization, Supervision, Writing -  
682 Review & Editing, Funding Acquisition; **G. Acien:** Conceptualization, Supervision, Writing - Review  
683 & Editing, Funding Acquisition.

#### 684 **Acknowledgements**

685 This research was funded by the H2020 Research and Innovation Programme under the Marie  
686 Sklodowska-Curie grant agreement (project: Digitalgaesation, 955520) and by the H2020 Research  
687 and Innovation Framework Programme (projects: PRODIGIO, 101007006; REALM, 101060991).  
688 Also, this work was supported by the Spanish Ministry of Science and Innovation (project:  
689 HYCO2BIO, PID2020-112709RB-C21). All the authors would like to thank the Institute for  
690 Agricultural and Fisheries Research and Training (IFAPA).

#### 691 **References**

- 692 Abdel-Raouf, N., Al-Homaidan, A.A., Ibraheem, I.B.M., 2012. Microalgae and wastewater treatment. Saudi J  
693 Biol Sci. <https://doi.org/10.1016/j.sjbs.2012.04.005>
- 694 Acien, F.G., Ferná Ndez, J.M., Molina-Grima, E., 2014. Economics of Microalgae Biomass Production.
- 695 Angelakis, A.N., Gikas, P., 2014. Water reuse: Overview of current practices and trends in the world with  
696 emphasis on EU states, Water Utility Journal.
- 697 Antonino Baez, Joseph Shiloach, 2014. Effect of elevated oxygen concentration on bacteria, yeasts, and  
698 cells propagated for production of biological compounds. Microb Cell Fact 13.
- 699 Aparicio, S., González-Camejo, J., Seco, A., Borrás, L., Robles, Á., Ferrer, J., 2023. Integrated microalgae-  
700 bacteria modelling: application to an outdoor membrane photobioreactor (MPBR). Science of the  
701 Total Environment 884. <https://doi.org/10.1016/j.scitotenv.2023.163669>
- 702 Aparicio, S., Robles, Á., Ferrer, J., Seco, A., Borrás Falomir, L., 2022a. Assessing and modeling nitrite  
703 inhibition in microalgae-bacteria consortia for wastewater treatment by means of photo-

704 respirometric and chlorophyll fluorescence techniques. *Science of the Total Environment* 808.  
705 <https://doi.org/10.1016/j.scitotenv.2021.152128>

706 Aparicio, S., Robles, Á., Ferrer, J., Seco, A., Borrás Falomir, L., 2022b. Assessing and modeling nitrite  
707 inhibition in microalgae-bacteria consortia for wastewater treatment by means of photo-  
708 respirometric and chlorophyll fluorescence techniques. *Science of the Total Environment* 808.  
709 <https://doi.org/10.1016/j.scitotenv.2021.152128>

710 Barceló-Villalobos, M., Fernández-del Olmo, P., Guzmán, J.L., Fernández-Sevilla, J.M., Acien Fernández, F.G.,  
711 2019. Evaluation of photosynthetic light integration by microalgae in a pilot-scale raceway reactor.  
712 *Bioresour Technol* 280, 404–411. <https://doi.org/10.1016/j.biortech.2019.02.032>

713 Barreiro-Vescovo, S., González-Fernández, C., de Godos, I., 2021. Characterization of communities in a  
714 microalgae-bacteria system treating domestic wastewater reveals dominance of phototrophic and  
715 pigmented bacteria. *Algal Res* 59. <https://doi.org/10.1016/j.algal.2021.102447>

716 Bernard, O., Rémond, B., 2012. Validation of a simple model accounting for light and temperature effect on  
717 microalgal growth. *Bioresour Technol* 123, 520–527. <https://doi.org/10.1016/j.biortech.2012.07.022>

718 Buhr, H., O., Miller, S., B., 1983. A dynamic model of the high-rate algal-bacterial wastewater treatment  
719 pond. *Water Research* 17, 29–37.

720 Casagli, F., Zuccaro, G., Bernard, O., Steyer, J.P., Ficara, E., 2021. ALBA: A comprehensive growth model to  
721 optimize algae-bacteria wastewater treatment in raceway ponds. *Water Res* 190.  
722 <https://doi.org/10.1016/j.watres.2020.116734>

723 Costache, T.A., Gabriel Acien Fernandez, F., Morales, M.M., Fernández-Sevilla, J.M., Stamatini, I., Molina, E.,  
724 2013. Comprehensive model of microalgae photosynthesis rate as a function of culture conditions in  
725 photobioreactors. *Appl Microbiol Biotechnol* 97, 7627–7637. <https://doi.org/10.1007/s00253-013-5035-2>

726

727 Council Directive of May 1991 concerning urban waste water treatment, 1991.

728 Darvehei, P., Bahri, P.A., Moheimani, N.R., 2018. Model development for the growth of microalgae: A  
729 review. *Renewable and Sustainable Energy Reviews*. <https://doi.org/10.1016/j.rser.2018.08.027>

730 Denis Dochain, 2001. Bioproces control , in: Denis Dochain (Ed.), . Wiley-ISTE Series, pp. 52–56.

731 Droop, M.R., 1970. Vitamin B 12 and marine ecology. Continous culture as an approach to nutritional  
732 kinetics. *Journal of the Marine Biological Association of the United Kingdom* 48, 629–636.

733 Fernández Sevilla, J.M., Molina Grima, E., Perez Parra, J., Acien Fernández, F.G., Magán Cañadas, J.J., Friedi,  
734 T., 2006. New species of microalgae and its application for animal and human consumption and in the  
735 production of carotenoids. WO 2006/087405.

736 Fujita, K., Okada, K., Katahira, K., n.d. The Fisher information matrix: A tutorial for calculation for decision  
737 making models.

738 Gao, F., Han, L., 2012. Implementing the Nelder-Mead simplex algorithm with adaptive parameters.  
739 *Comput Optim Appl* 51, 259–277. <https://doi.org/10.1007/s10589-010-9329-3>

740 Grima, E.M., Camacho, F.G., Pérez, J.A.S., Sevilla, J.M.F., Fernández, F.G.A., Gómez, A.C., 1994. A  
741 mathematical model of microalgal growth in light-limited chemostat culture. *Journal of Chemical*  
742 *Technology & Biotechnology* 61, 167–173. <https://doi.org/10.1002/jctb.280610212>

743 Grivalský, T., Ranglová, K., da Câmara Manoel, J.A., Lakatos, G.E., Lhotský, R., Masojídek, J., 2019.  
744 Development of thin-layer cascades for microalgae cultivation: milestones (review). *Folia Microbiol*  
745 (Praha). <https://doi.org/10.1007/s12223-019-00739-7>

746 Henze, Mogens., Gujer, Willi., Mino, Takashi., Van Loosdrecht, Mark., 2000. Activated sludge models ASM1,  
747 ASM2, ASM2d and ASM3. IWA Pub.

748 Ippoliti, D., Gómez, C., del Mar Morales-Amaral, M., Pistocchi, R., Fernández-Sevilla, J.M., Acién, F.G., 2016.  
749 Modeling of photosynthesis and respiration rate for *Isochrysis galbana* (T-Iso) and its influence on the  
750 production of this strain. *Bioresour Technol* 203, 71–79.  
751 <https://doi.org/10.1016/j.biortech.2015.12.050>

752 Lee, E., Jalalizadeh, M., Zhang, Q., 2015. Growth kinetic models for microalgae cultivation: A review. *Algal*  
753 *Res.* <https://doi.org/10.1016/j.algal.2015.10.004>

754 Masojídek, J., Gómez-Serrano, C., Ranglová, K., Cicchi, B., Encinas Bogeat, Á., Câmara Manoel, J.A., Sanches  
755 Zurano, A., Silva Benavides, A.M., Barceló-Villalobos, M., Robles Carnero, V.A., Ördög, V., Gómez  
756 Pinchetti, J.L., Vörös, L., Arbib, Z., Rogalla, F., Torzillo, G., Lopez Figueroa, F., Acién-Fernández, F.G.,  
757 2022. Photosynthesis Monitoring in Microalgae Cultures Grown on Municipal Wastewater as a  
758 Nutrient Source in Large-Scale Outdoor Bioreactors. *Biology (Basel)* 11.  
759 <https://doi.org/10.3390/biology11101380>

760 Mohd Udaiyappan, A.F., Abu Hasan, H., Takriff, M.S., Sheikh Abdullah, S.R., 2017. A review of the  
761 potentials, challenges and current status of microalgae biomass applications in industrial wastewater  
762 treatment. *Journal of Water Process Engineering.* <https://doi.org/10.1016/j.jwpe.2017.09.006>

763 Monod, J., 1949. THE GROWTH OF BACTERIAL CULTURES.

764 Morillas-España, A., Lafarga, T., Acién-Fernández, F.G., Gómez-Serrano, C., González-López, C.V., 2021a.  
765 Annual production of microalgae in wastewater using pilot-scale thin-layer cascade photobioreactors.  
766 *J Appl Phycol* 33, 3861–3871. <https://doi.org/10.1007/s10811-021-02565-2>

767 Morillas-España, A., Lafarga, T., Gómez-Serrano, C., Acién-Fernández, F.G., González-López, C.V., 2020.  
768 Year-long production of *Scenedesmus almeriensis* in pilot-scale raceway and thin-layer cascade  
769 photobioreactors. *Algal Res* 51. <https://doi.org/10.1016/j.algal.2020.102069>

770 Morillas-España, A., Lafarga, T., Sánchez-Zurano, A., Gabriel Acién-Fernández, F., Rodríguez-Miranda, E.,  
771 Gómez-Serrano, C., Cynthia, & González-López, V., 2021b. Year-long evaluation of microalgae  
772 production in wastewater using pilot-scale raceway photobioreactors: Assessment of biomass  
773 productivity and nutrient recovery capacity.

774 Muñoz, I.L., Bernard, O., 2021. Modeling the influence of temperature, light intensity and oxygen  
775 concentration on microalgal growth rate. *Processes* 9. <https://doi.org/10.3390/pr9030496>

776 Muñoz, R., Guieysse, B., 2006. Algal-bacterial processes for the treatment of hazardous contaminants: A  
777 review. *Water Res.* <https://doi.org/10.1016/j.watres.2006.06.011>

778 Ncr, (, Clinton, J., 1999. CRISP-DM 1.0 Step-by-step data mining guide. DaimlerChrysler.

779 Nordio, R., Delgado, F.J., Sánchez-Zurano, A., Hernandez, J.G., Rodríguez-Miranda, E., Guzmán, J.L., Lafarga,  
780 T., Acién, G., 2023. Long-term assessment of the nutrient recovery capacity and biomass productivity  
781 of *Scenedesmus almeriensis* in raceway reactors using unprocessed urban wastewater. *Bioresour*  
782 *Technol* 369. <https://doi.org/10.1016/j.biortech.2022.128374>

- 783 Pasztor I., Thury P., Pulai J., 2009. Chemical oxygen demand fractions of municipal wastewater for modeling  
784 of wastewater treatment. *International Journal of Environmental Science and Technology* 6, 51–56.
- 785 Posadas, E., Morales, M. del M., Gomez, C., Ación, F.G., Muñoz, R., 2015. Influence of pH and CO<sub>2</sub> source on  
786 the performance of microalgae-based secondary domestic wastewater treatment in outdoors pilot  
787 raceways. *Chemical Engineering Journal* 265, 239–248. <https://doi.org/10.1016/j.cej.2014.12.059>
- 788 Rossi, S., Bellucci, M., Marazzi, F., Mezzanotte, V., Ficara, E., 2018. Activity assessment of microalgal-  
789 bacterial consortia based on respirometric tests. *Water Science and Technology* 78, 207–215.  
790 <https://doi.org/10.2166/wst.2018.078>
- 791 Rossi, S., Casagli, F., Mantovani, M., Mezzanotte, V., Ficara, E., 2020a. Selection of photosynthesis and  
792 respiration models to assess the effect of environmental conditions on mixed microalgae consortia  
793 grown on wastewater. *Bioresour Technol* 305. <https://doi.org/10.1016/j.biortech.2020.122995>
- 794 Rossi, S., Casagli, F., Mantovani, M., Mezzanotte, V., Ficara, E., 2020b. Selection of photosynthesis and  
795 respiration models to assess the effect of environmental conditions on mixed microalgae consortia  
796 grown on wastewater. *Bioresour Technol* 305. <https://doi.org/10.1016/j.biortech.2020.122995>
- 797 Sánchez Zurano, A., Garrido Cárdenas, J.A., Gómez Serrano, C., Morales Amaral, M., Ación-Fernández, F.G.,  
798 Fernández Sevilla, J.M., Molina Grima, E., 2020. Year-long assessment of a pilot-scale thin-layer  
799 reactor for microalgae wastewater treatment. Variation in the microalgae-bacteria consortium and  
800 the impact of environmental conditions. *Algal Res* 50. <https://doi.org/10.1016/j.algal.2020.101983>
- 801 Sánchez Zurano, A., Gómez Serrano, C., Ación-Fernández, F.G., Fernández-Sevilla, J.M., Molina-Grima, E.,  
802 2021. Modeling of photosynthesis and respiration rate for microalgae–bacteria consortia. *Biotechnol*  
803 *Bioeng* 118, 952–962. <https://doi.org/10.1002/bit.27625>
- 804 Sánchez-Zurano, A., Gómez-Serrano, C., Ación-Fernández, F.G., Fernández-Sevilla, J.M., Molina-Grima, E.,  
805 2020. A novel photo-respirometry method to characterize consortia in microalgae-related wastewater  
806 treatment processes. *Algal Res* 47. <https://doi.org/10.1016/j.algal.2020.101858>
- 807 Sánchez-zurano, A., Rodríguez-miranda, E., Guzmán, J.L., Ación-fernández, F.G., Fernández-sevilla, J.M.,  
808 Grima, E.M., 2021. Abaco: A new model of microalgae-bacteria consortia for biological treatment of  
809 wastewaters. *Applied Sciences (Switzerland)* 11, 1–24. <https://doi.org/10.3390/app11030998>
- 810 Solimeno, A., García, J., 2017. Microalgae-bacteria models evolution: From microalgae steady-state to  
811 integrated microalgae-bacteria wastewater treatment models – A comparative review. *Science of the*  
812 *Total Environment*. <https://doi.org/10.1016/j.scitotenv.2017.07.114>
- 813 Solimeno, A., Gómez-Serrano, C., Ación, F.G., 2019. BIO\_ALGAE 2: improved model of microalgae and  
814 bacteria consortia for wastewater treatment. *Environmental Science and Pollution Research* 26,  
815 25855–25868. <https://doi.org/10.1007/s11356-019-05824-5>
- 816 Solovchenko, A.E., Ismagulova, T.T., Lukyanov, A.A., Vasilieva, S.G., Konyukhov, I. V., Pogosyan, S.I.,  
817 Lobakova, E.S., Gorelova, O.A., 2019. Luxury phosphorus uptake in microalgae. *J Appl Phycol*.  
818 <https://doi.org/10.1007/s10811-019-01831-8>
- 819 Strosser, P., Dworak, T., Andrés Garzon Delvaux, P., Berglund, M., Schmidt, G., Mysiak, J., Kossida, M.,  
820 Iacovides, I., Ashton, V., Seiz Puyuelo, R., De Paoli, G., Stanley, K., 2012. Gap Analysis of the Water  
821 Scarcity and Droughts Policy in the EU Final Report Gap Analysis of the Water Scarcity and Droughts  
822 Policy in the EU European Commission.



823 Zambrano, J., Krustok, I., Nehrenheim, E., Carlsson, B., 2016. A simple model for algae-bacteria interaction  
824 in photo-bioreactors.

825 Zurano, A.S., Serrano, C.G., Acién-Fernández, F.G., Fernández-Sevilla, J.M., Molina-Grima, E., 2021.  
826 Modelling of photosynthesis, respiration, and nutrient yield coefficients in Scenedemus  
827 almeriensis culture as a function of nitrogen and phosphorus. Appl Microbiol Biotechnol 105,  
828 7487–7503. <https://doi.org/10.1007/s00253-021-11484-8>

829 **Tables**

830 Table 1.- ABACO-2 model process rates

n.	Process	Process rate [ $\text{g}\cdot\text{m}^{-3}\cdot\text{day}^{-1}$ ]
1	Microalgae growth on $\text{NH}_4$	$\mu_{max,alg} \cdot \mu(I_{av}) \cdot \overline{\mu(T)} \cdot \overline{\mu(pH)} \cdot \overline{\mu(O_2)}_{alg} \cdot \overline{\mu(N - NH_4)} \cdot \overline{\mu(P - PO_4)} \cdot X_{alg}$
2	Microalgae growth on $\text{NO}_3$	$\mu_{max,alg} \cdot \mu(I_{av}) \cdot \overline{\mu(T)} \cdot \overline{\mu(pH)} \cdot \overline{\mu(O_2)}_{alg} \cdot \overline{\mu(N - NO_3)} \cdot \overline{\mu(P - PO_4)} \cdot (1 - \overline{\mu(N - NH_4)}) \cdot X_{alg}$
3	Microalgae decay	$m \cdot X_{alg}$
4	Nitrifying bacteria growth	$\mu_{max,nit} \cdot \overline{\mu_{nit}(T)} \cdot \overline{\mu_{nit}(pH)} \cdot \overline{\mu_{nit}(O_2)} \cdot \overline{\mu_{nit}(N - NH_4)} \cdot X_{nit}$
5	Nitrifying bacteria decay	$\theta_{nit} \cdot m_{nit} \cdot X_{nit}$
6	Heterotrophic bacteria growth	$\mu_{max,het} \cdot \overline{\mu_{het}(T)} \cdot \overline{\mu_{het}(pH)} \cdot \overline{\mu_{het}(O_2)} \cdot \overline{\mu_{het}(N - NH_4)} \cdot \overline{\mu_{het}(BSMO)} \cdot X_{het}$
7	Heterotrophic bacteria decay	$\theta_{het} \cdot m_{het} \cdot X_{het}$

831

832 Table 2.- ABACO-2 stoichiometric matrix

Component	→ i	$\text{S}_{\text{NH}_4}$	$\text{S}_{\text{NO}_3}$	$\text{S}_{\text{PO}_4}$	$\text{S}_{\text{BSMO}}$	$\text{S}_{\text{O}_2}$	$X_{alg}$	$X_{nit}$	$X_{het}$
j Process	↓	$[\text{g}_{\text{NH}_4}\cdot\text{m}^{-3}]$	$[\text{g}_{\text{NO}_3}\cdot\text{m}^{-3}]$	$[\text{g}_{\text{PO}_4}\cdot\text{m}^{-3}]$	$[\text{g}_{\text{BSMO}}\cdot\text{m}^{-3}]$	$[\text{g}_{\text{O}_2}\cdot\text{m}^{-3}]$	$[\text{g}_{alg}\cdot\text{m}^{-3}]$	$[\text{g}_{nit}\cdot\text{m}^{-3}]$	$[\text{g}_{het}\cdot\text{m}^{-3}]$
1	Microalgae growth on $\text{NH}_4$	$-Y_{\text{NH}_4,alg}$		$-Y_{\text{PO}_4,alg}$		$+Y_{\text{O}_2,alg}$	1		
2	Microalgae growth on $\text{NO}_3$		$-Y_{\text{NO}_3,alg}$	$-Y_{\text{PO}_4,alg}$		$+Y_{\text{O}_2,alg}$	1		
3	Microalgae endogenous respiration				$1 - f_{alg}$	$-Y_{\text{O}_2,alg}$	-1		
4	Nitrifying bacteria growth	$-Y_{\text{NH}_4,nit}$	$+Y_{\text{NO}_3,nit}$			$-Y_{\text{O}_2,nit}$		1	
5	Nitrifying bacteria decay				$1 - f_{bac}$			-1	
6	Heterotrophic bacteria growth	$-Y_{\text{NH}_4,het}$			$-Y_{\text{BSMO}}$	$-Y_{\text{O}_2,het}$			1
7	Heterotrophic bacteria decay				$1 - f_{bac}$				-1

833

834

835

836  
837  
838  
839  
840  
841  
842

Table 3.- Stoichiometric coefficients.

Parameter	Value	Units	Source
$Y_{NH_4,nit}$	7.9	$g_{NH_4} \cdot g_{nit}^{-1}$	(Henze et al., 2000)
$Y_{NO_3,nit}$	26.7	$g_{NO_3} \cdot g_{nit}^{-1}$	(Henze et al., 2000)
$Y_{NH_4,het}$	0.16	$g_{NH_4} \cdot g_{het}^{-1}$	(Henze et al., 2000)
$Y_{BSMO}$	2.3	$g_{BSMO} \cdot g_{het}^{-1}$	(Henze et al., 2000)
$Y_{O_2,alg}$	1.33	$g_{O_2} \cdot g_{alg}^{-1}$	
$Y_{O_2,nit}$	12.44	$g_{O_2} \cdot g_{nit}^{-1}$	(Henze et al., 2000)
$Y_{O_2,het}$	0.4	$g_{O_2} \cdot g_{het}^{-1}$	(Henze et al., 2000)
$f_{alg}$	0.1	–	(Solimeno et al., 2019)
$f_{bac}$	0.1	–	(Solimeno et al., 2019)
$\theta_{het}$	1.07	$^{\circ}C$	(Casagli et al., 2021)
$\theta_{nit}$	1.1	$^{\circ}C$	(Casagli et al., 2021)

843  
844

Table 4.- Microalgae kinetic parameters.

Parameter	Value	Units	Source
Microalgae kinetic parameters			
$I_K$	168	$\mu E \cdot m^{-2} \cdot s^{-1}$	(Sánchez Zurano et al., 2021)
$n$	1.7	–	(Sánchez Zurano et al., 2021)
$K_a$	0.08	$m^2 g^{-1}$	This study
$I_{K_r}$	134	$\mu E \cdot m^{-2} \cdot s^{-1}$	(Sánchez Zurano et al., 2021)
$n_r$	1.4	–	(Sánchez Zurano et al., 2021)
$T_{min,alg}$	-10	$^{\circ}C$	(Casagli et al., 2021)

$T_{max,alg}$	38	°C	(Casagli et al., 2021)
$T_{opt,alg}$	20	°C	(Casagli et al., 2021)
$pH_{min,alg}$	1.8	–	(Sánchez Zurano et al., 2021)
$pH_{max,alg}$	12.9	–	(Sánchez Zurano et al., 2021)
$pH_{opt,alg}$	8.5	–	(Sánchez Zurano et al., 2021)
$S_{O_2,max}$	22.68	$g_{O_2} \cdot m^{-3}$	(Sánchez Zurano et al., 2021)
$z$	4.15	–	(Sánchez Zurano et al., 2021)
$K_{S,N-NH_4,alg}$	1.54	$g_{N-NH_4} \cdot m^{-3}$	(Zurano et al., 2021)
$K_{i,N-NH_4,alg}$	571	$g_{N-NH_4} \cdot m^{-3}$	(Zurano et al., 2021)
$n_{N-NH_4,alg}$	2	-	(Zurano et al., 2021)
$K_{S,N-NO_3,alg}$	2.77	$g_{N-NO_3} \cdot m^{-3}$	(Zurano et al., 2021)
$K_{i,N-NO_3,alg}$	387	$g_{N-NO_3} \cdot m^{-3}$	(Zurano et al., 2021)
$n_{N-NO_3,alg}$	2	–	(Zurano et al., 2021)
$K_{S,P-PO_4,alg}$	0.43	$g_{P-PO_4} \cdot m^{-3}$	(Zurano et al., 2021)

---

Heterotrophic bacteria kinetic parameters

$T_{min,het}$	-3	°C	(Casagli et al., 2021)
$T_{max,het}$	42	°C	(Casagli et al., 2021)
$T_{opt,het}$	25	°C	(Casagli et al., 2021)
$pH_{min,het}$	6	–	(Sánchez Zurano et al., 2021)
$pH_{max,het}$	12	–	(Sánchez Zurano et al., 2021)
$pH_{opt,het}$	9	–	(Sánchez Zurano et al., 2021)
$K_{S,O_2,het}$	1.98	$g_{O_2} \cdot m^{-3}$	(Sánchez Zurano et al., 2021)
$K_{S,N-NH_4,het}$	0.5	$g_{N-NH_4} \cdot m^{-3}$	(Henze et al., 2000)
$K_{S,BSMO,het}$	0.299	$g_{BSMO} \cdot m^{-3}$	(Henze et al., 2000)

---

Nitrifying bacteria kinetic parameters

$T_{min,nit}$	-8	°C	(Casagli et al., 2021)
$T_{max,nit}$	38	°C	(Casagli et al., 2021)

$T_{opt,nit}$	20	$^{\circ}C$	(Casagli et al., 2021)
$pH_{min,nit}$	2	–	(Sánchez Zurano et al., 2021)
$pH_{max,nit}$	13.4	–	(Sánchez Zurano et al., 2021)
$pH_{opt,nit}$	9	–	(Sánchez Zurano et al., 2021)
$K_{S,O_2,nit}$	1.080	$g_{O_2} \cdot m^{-3}$	(Henze et al., 2000)
$K_{S,O_2,nit}$	104.9	$g_{O_2} \cdot m^{-3}$	(Henze et al., 2000)
$K_{S,N-NH_4,nit}$	1	$g_{N-NH_4} \cdot m^{-3}$	(Henze et al., 2000)

---

846 Table 5.- Microalgae nutrient yield parameters.

Parameter	Value	Units	Source	Parameter	Value	Units	Source	Parameter	Value	Units	Source
$Y_{NH_4,max}$	0.4	$g_{N-NH_4} \cdot g_{alg}$	Calibrated	$Y_{NO_3,max}$	0.1	$g_{N-NO_3} \cdot g_{alg}$	Calibrated	$Y_{PO_4,max}$	0.003	$g_{P-PO_4} \cdot g_{alg}$	Calibrated
$K_{S,NH_4}$	25	-	(Zuran o et al., 2021)	$K_{S,NO_3}$	25	-	(Zurano et al., 2021)	$K_{S,PO_4}$	3.2	-	(Zurano et al., 2021)
$t_{NH_4}$	2	-		$t_{NO_3}$	2	-		$t_{PPO_4}$	2.14	-	
$NH_{4,max}$	80	$g_{N-NH_4} \cdot m^{-3}$		$NO_{3,max}$	80	$g_{N-NO_3} \cdot m^{-3}$		$PO_{4,max}$	22	$g_{P-PO_4} \cdot m^{-3}$	
$NH_{4,min}$	10	$g_{N-NH_4} \cdot m^{-3}$		$NO_{3,min}$	10	$g_{N-NO_3} \cdot m^{-3}$		$PO_{4,min}$	2	$g_{P-PO_4} \cdot m^{-3}$	
$NH_{4,opt}$	55	$g_{N-NH_4} \cdot m^{-3}$		$NO_{3,opt}$	55	$g_{N-NO_3} \cdot m^{-3}$		$PO_{4,opt}$	15	$g_{P-PO_4} \cdot m^{-3}$	

847

848

849 Table 6.- List of calibrated parameters and their corresponding values

Parameter	Description	Value	Units
$\mu_{max,alg}$	Maximum algal growth rate	1.5	$day^{-1}$
$m_{min}$	Minimum algal respiration rate	0.1	$day^{-1}$
$m_{max}$	Maximum algal respiration rate	0.008	$day^{-1}$
$\mu_{max,nit}$	Maximum nitrifying bacteria growth rate	0.75	$day^{-1}$
$m_{nit}$	Nitrifying bacteria decay	$0.05 \mu_{max,nit}$	$day^{-1}$
$\mu_{max,het}$	Maximum heterotrophic bacteria growth rate	3.4	$day^{-1}$
$m_{het}$	Heterotrophic bacteria decay	$0.2 \mu_{max,het}$	$day^{-1}$
$Y_{NH_4,max}$	$NH_4^+$ microalage nutrient yield max	0.6	$g_{NH_4} \cdot g_{alg}^{-1}$
$Y_{NO_3,max}$	$NO_3^-$ microalage nutrient yield max	0.1	$g_{NO_3} \cdot g_{alg}^{-1}$
$Y_{PO_4,max}$	$PO_4^{3-}$ microalage nutrient yield max	0.004	$g_{PO_4} \cdot g_{alg}^{-1}$
$Kl_a$	$O_2$ natural mass transfer	0.1	$h^{-1}$
$\alpha$	Nutrient assimilation coefficient	1	-

850

851 Table 7.- List of most sensible parameters

Parameter	Units	Nominal value	Standard deviation	Most affected parameters
$I_k$	$\mu E \cdot m^{-2} \cdot s^{-1}$	168	0.02	$X_{alg}, X_{het}, X_{nit}, S_{NH_4}, S_{NO_3}, S_{PO_4}, S_{BSMO}, S_{O_2}$
$K_a$	$m^2 g^{-1}$	0.08	1.4E-5	$X_{alg}, X_{het}, X_{nit}, S_{NH_4}, S_{NO_3}, S_{PO_4}, S_{BSMO}, S_{O_2}$
$n$	–	1.7	1.6E-4	$X_{alg}, X_{het}, X_{nit}, S_{NO_3}, S_{PO_4}, S_{O_2}$
$\mu_{max,alg}$	$day^{-1}$	1.5	5.38E-4	$X_{alg}, X_{het}, X_{nit}, S_{NH_4}, S_{NO_3}, S_{PO_4}, S_{BSMO}, S_{O_2}$
$\mu_{max,het}$	$day^{-1}$	3.4	0.0016	$X_{het}, S_{BSMO}$
$\mu_{max,nit}$	$day^{-1}$	0.75	0.0004	$X_{nit}, S_{NO_3}, S_{NH_4}$
$m_{min}$	$day^{-1}$	0.1	8E-6	$X_{alg}, X_{het}, X_{nit}, S_{NO_3}, S_{BSMO}, S_{O_2}$
$m_{nit}$	$day^{-1}$	0.05 $\mu_{max,nit}$	8.34E-5	$X_{het}, X_{nit}, S_{NO_3}, S_{BSMO}$ ,
$m_{het}$	$day^{-1}$	0.2 $\mu_{max,het}$	6.8E-5	$X_{het}, X_{nit}, S_{NO_3}, S_{BSMO}$ ,
$O_{2,max}$	$mg_{O_2} \cdot l^{-1}$	22.68	0.0011	$X_{alg}, X_{het}, X_{nit}, S_{NO_3}, S_{PO_4}, S_{BSMO}, S_{O_2}$
$Y_{NH_4,max}$	–	0.6	0.001	$X_{het}, X_{nit}, S_{NH_4}, S_{NO_3}$
$Y_{NH_4,nit}$	–	0.4	0.016	$X_{nit}, S_{NH_4}$
$Y_{NO_3,nit}$	–	26.76	0.11	$S_{NO_3}$
Cardinal parameters	Units	Opt, max, min	Standard deviation	Most affected parameters
$T_{alg}$	$^{\circ}C$	38,20,-10	0.0026	$X_{alg}, X_{het}, X_{nit}, S_{NH_4}, S_{NO_3}, S_{PO_4}, S_{BSMO}, S_{O_2}$
$pH_{alg}$	–	8.5, 12.9, 1.8	0.0032	$X_{alg}, X_{het}, X_{nit}, S_{NH_4}, S_{NO_3}, S_{PO_4}, S_{BSMO}, S_{O_2}$
$T_{nit}$	$^{\circ}C$	20,38,-8	0.04	$X_{het}, X_{nit}, S_{NH_4}, S_{NO_3}, S_{BSMO}$
$pH_{nit}$	–	9, 13.4, 2	0.024	$X_{het}, X_{nit}, S_{NH_4}, S_{NO_3}, S_{BSMO}$
$T_{het}$	$^{\circ}C$	25,42,-3	0.034	$X_{het}, X_{nit}, S_{NO_3}, S_{BSMO}$
$pH_{het}$	–	9, 12, 6	0.0026	$X_{het}, X_{nit}, S_{NO_3}, S_{BSMO}$

852

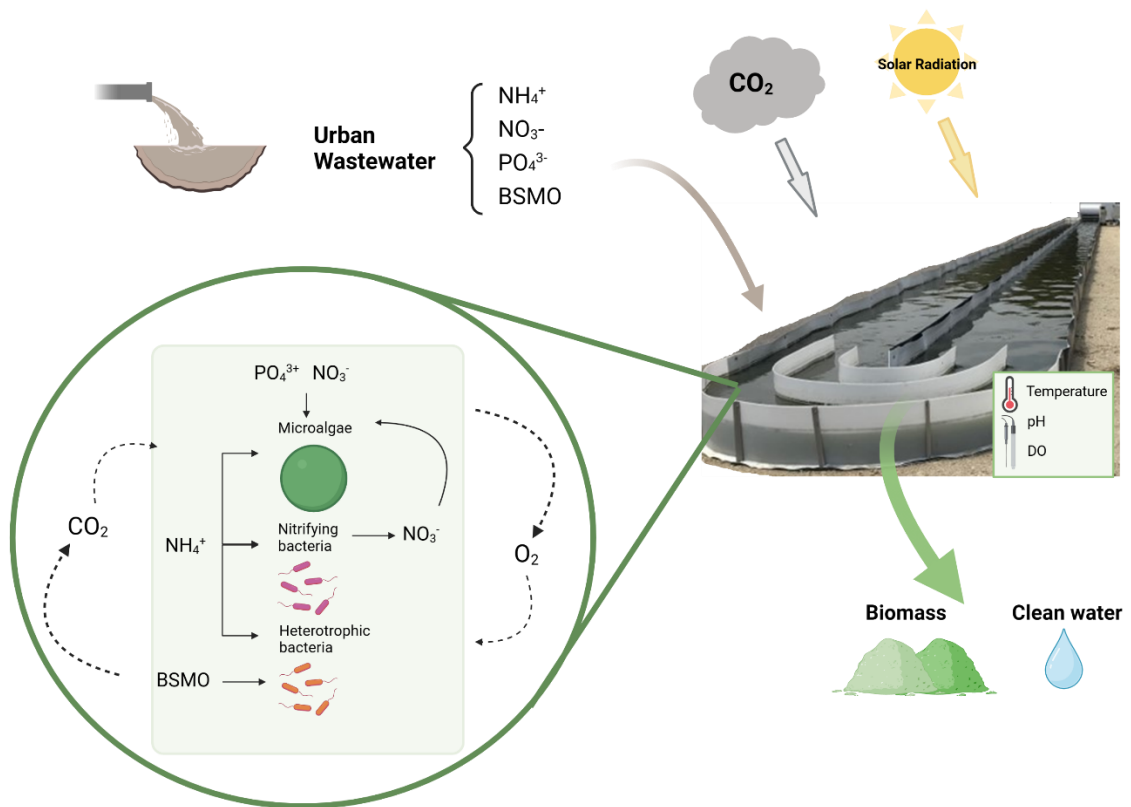
853

854 Table 8.- Validation errors of the ABACO-2 model.

Parameter	NRMSE	TIC
$X_{tot} [g \cdot m^{-3}]$	0.21	0.16
$S_{NH_4} [g \cdot m^{-3}]$	0.22	0.55
$S_{NO_3} [g \cdot m^{-3}]$	0.15	0.21
$S_{PO_4} [g \cdot m^{-3}]$	0.23	0.24
$S_{BSMO} [g \cdot m^{-3}]$	0.21	0.2
$S_{O_2} [g \cdot m^{-3}]$	0.14	0.21

855

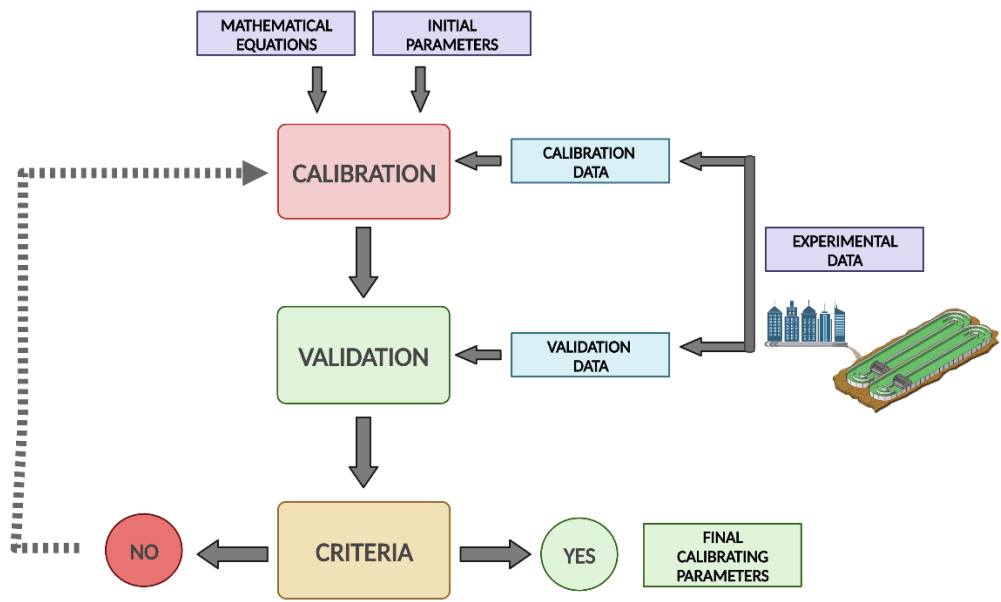
856 **Figures**



857

858 Figure 1.- Schematic description of the biological mechanisms taking in place in microalgae-bacteria  
859 wastewater systems.

860



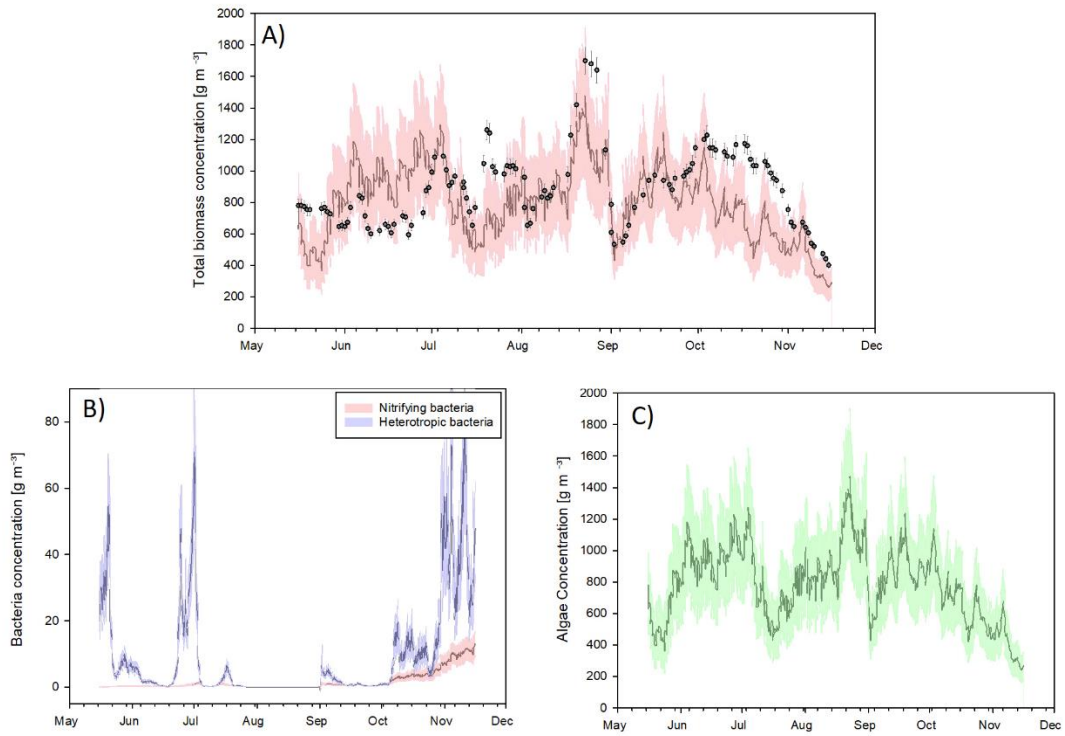
861

862

Figure 2.- Calibration methodology used in the present work.

863

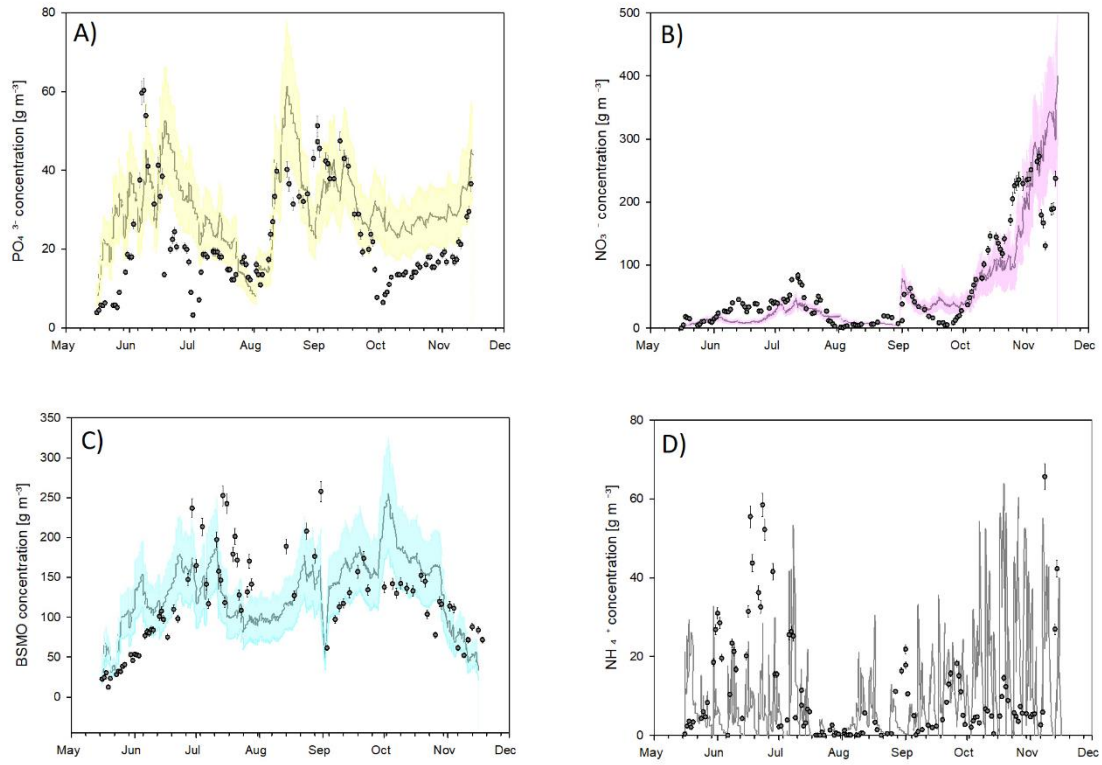




864

865 Figure 3.- Biomass concentration evolution. A) Total biomass concentration (sum of algae and bacteria,  
 866 simulated (continuous line) and experimental (scatter plot); B) Nitrifying and heterotrophic concentration; C)  
 867 Algae concentration. The model shade is the model confidence interval at 95%.

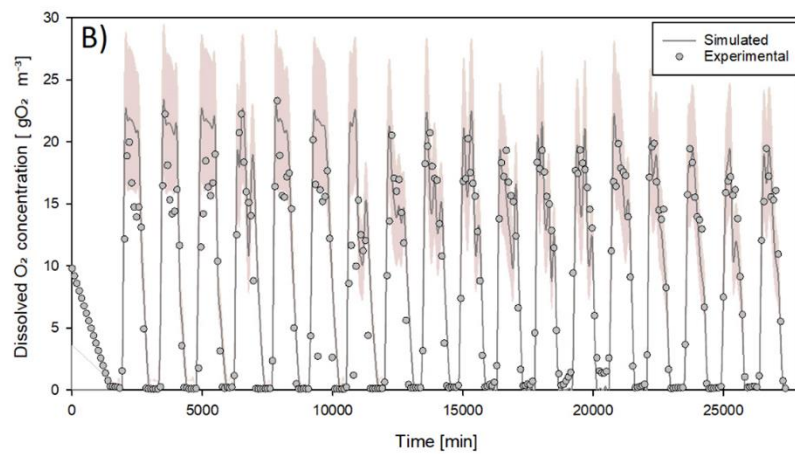
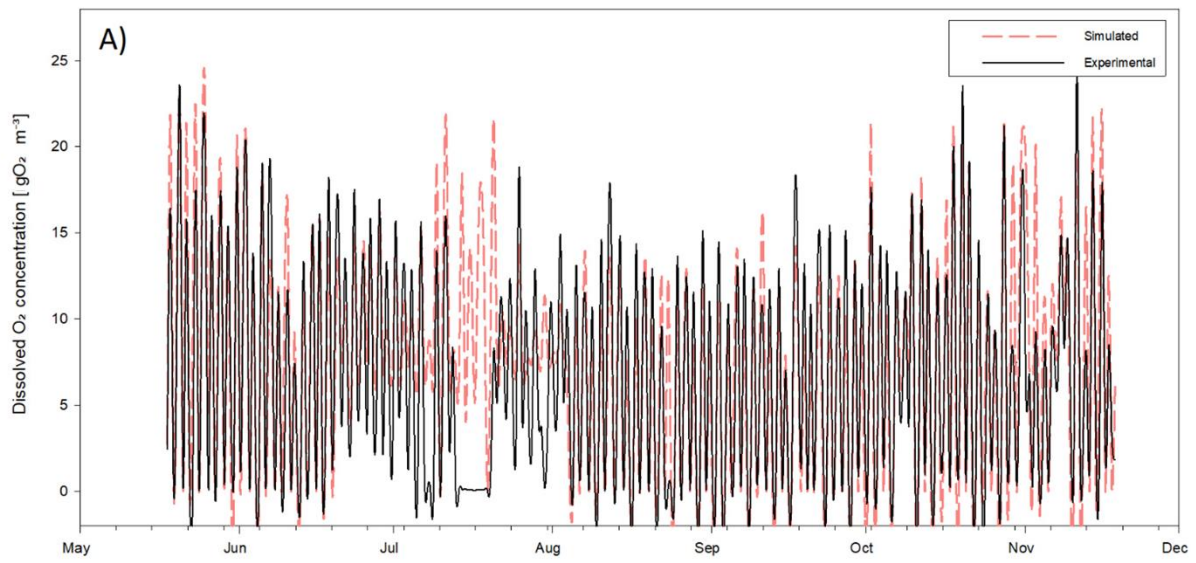
868



869

870 Figure 4.- Variation of culture nutrients A)  $\text{PO}_4^{3-}$ , B)  $\text{NO}_3^-$ , C)  $\text{NH}_4^+$  and D) BSMO concentration, in  $\text{g}\cdot\text{m}^{-3}$   
 871 respectively (experimental, scatter plot; model prediction, continuous line).

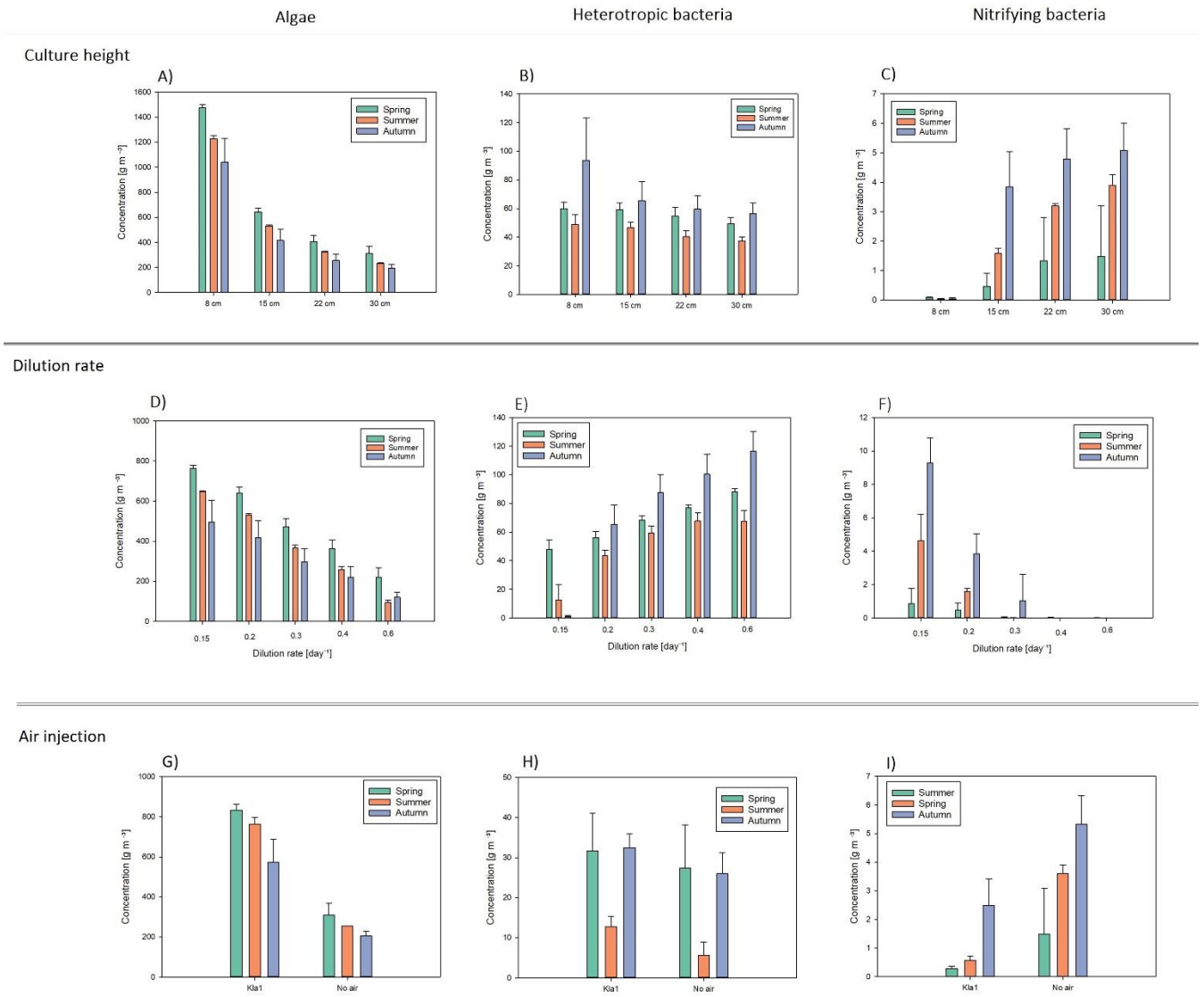
872



873

874 Figure 5.- Simulation of the dissolved oxygen in the culture. A) Experimental and simulated dissolved  
 875 oxygen along the entire study period, B) Representation of the oxygen in a shorter period.

876



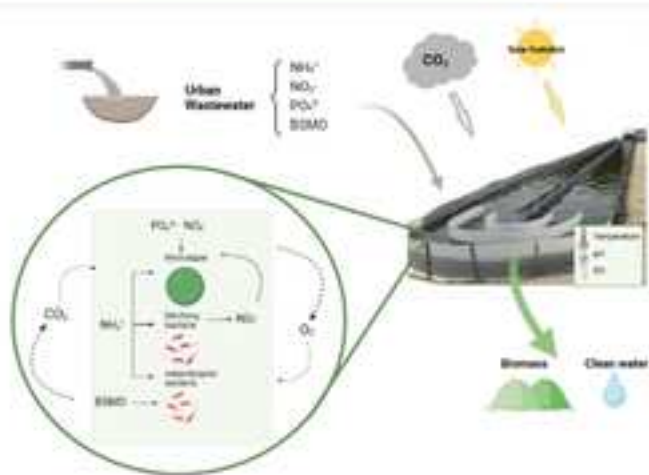
877

878 Figure 6: Application of ABACO-2 model in a case-study. Algae, heterotropic and nitrifying bacteria  
 879 concentration evolution depending on: A), B), C) culture height; D), E), F) Dilution rate; G), H), I) with or  
 880 without injecting air into the system

881

882

Define the biological system



Model development

Calibration of parameters

Validation

Process rate [ $\text{g m}^{-3} \text{ day}^{-1}$ ]	
$\rho_1$	$\rho_{max} \frac{K_1 X}{K_1 + X} \frac{\mu(T) \mu(\text{pH}) (1 - (\frac{X}{X_{max}})^n)}{1 + X}$
$\rho_2$	$\theta_{max} \cdot m \cdot X$
.....	
$\rho_n$	

